A Spectral Cumulus Parameterization Scheme Interpolating between Two Convective Updrafts with Semi-Lagrangian Calculation of Transport by Compensatory Subsidence

HIROMASA YOSHIMURA AND RYO MIZUTA

Meteorological Research Institute, Tsukuba, Japan

HIROYUKI MURAKAMI

NOAA/Geophysical Fluid Dynamics Laboratory, Princeton University, Princeton, New Jersey

(Manuscript received 18 February 2014, in final form 18 September 2014)

ABSTRACT

The authors have developed a new spectral cumulus parameterization scheme that explicitly considers an ensemble of multiple convective updrafts by interpolating in-cloud variables between two convective updrafts with large and small entrainment rates. This cumulus scheme has the advantages that the variables in entraining and detraining convective updrafts are calculated in detail layer by layer as in the Tiedtke scheme, and that a spectrum of convective updrafts with different heights due to the difference in entrainment rates is explicitly represented, as in the Arakawa–Schubert scheme. A conservative and monotonic semi-Lagrangian scheme is used for calculation of transport by convection-induced compensatory subsidence. Use of the semi-Lagrangian scheme relaxes the mass-flux limit due to the Courant–Friedrichs–Lewy (CFL) condition, and moreover ensures nonnegative natural material transport. A global atmospheric model using this cumulus scheme gives an atmospheric simulation that agrees well with the observational climatology.

1. Introduction

Cumulus parameterization schemes are used in atmospheric models at horizontal resolutions of about 5 km or coarser (e.g., Mizuta et al. 2006; Kanada et al. 2008) so that the effect of subgrid-scale cumulus clouds can be taken into consideration. Simulations by models at horizontal resolutions from 1 to 3 km have some success without cumulus schemes (e.g., Lilly 1990; Posselt et al. 2008; Satoh et al. 2008; Eito et al. 2010). However, horizontal resolution on the order of 100 m is necessary to resolve individual cumulus clouds explicitly (Yamasaki 1975; Bryan et al. 2003). Thus, cumulus parameterizations are still important even now as the resolution of atmospheric models improves.

Various cumulus parameterization schemes have been developed, such as convective-adjustment schemes (e.g., Manabe and Strickler 1964; Betts and Miller 1986), Kuo schemes (Kuo 1965, 1974), and mass-flux schemes. Mass-flux schemes are widely used because they explicitly calculate subgrid-scale convective updraft and downdraft mass fluxes, and are suitable for calculation of convective transport of material.

Traditional mass-flux schemes are classified into two main types: the Arakawa–Schubert (AS) type using the simple spectral cloud model approach and the Tiedtke type using the bulk cloud model approach. There are also other types of schemes, such as the one that represents the cloud spectrum explicitly with buoyancy sorting (e.g., Emanuel 1991; Hu 1997; Raymond and Blyth 1986). The AS-type schemes (e.g., Arakawa and Schubert 1974; Moorthi and Suarez 1992; Pan and Randall 1998; Zhang and McFarlane 1995) explicitly calculate multiple convective updrafts with different heights due to differences in entrainment rates. However, they calculate each individual convective updraft as a simple entraining plume to reduce the computational cost. They calculate the values of in-cloud variables (e.g., moist static energy and water vapor) at the cloud top of the updraft from those at the cloud bottom without explicitly calculating the values at intermediate levels. In contrast, the Tiedtke-type schemes (e.g., Tiedtke 1989; Nordeng 1994; Gregory and Rowntree 1990; Kain and Fritsch 1990; Bechtold et al. 2008) calculate only

Corresponding author address: Hiromasa Yoshimura, Meteorological Research Institute, 1-1 Nagamine, Tsukuba 305-0052, Japan. E-mail: hyoshimu@mri-jma.go.jp

DOI: 10.1175/MWR-D-14-00068.1

one convective updraft, but calculate it as a more elaborate entraining and detraining plume. They calculate the in-cloud variables layer by layer from the cloud bottom to the cloud top. Thus, the Tiedtke-type schemes and the AS-type schemes each have their own advantages.

One way to combine the advantages of the AS and Tiedtke types is to calculate individual multiple convective updrafts explicitly and at the same time to calculate the values of in-cloud variables layer by layer from the cloud bottom to the cloud top (e.g., Nober and Graf 2005; Chikira and Sugiyama 2010; Wagner and Graf 2010). It is a good way, but the computational cost is high because of the need to calculate explicitly about 10 or more convective updrafts layer by layer. Moreover, the greater the number of vertical levels, the greater the number of convective updrafts needed to obtain a smooth distribution of cloud-top levels.

In this study, we have developed a new cumulus scheme that has the advantages of both AS and Tiedtke types, and moreover has low computational cost. The scheme represents multiple convective updrafts with different entrainment rates by calculating only two convective updrafts with large and small entrainment rates and interpolating the in-cloud variables between the two updrafts. The new scheme has been implemented in a global atmospheric model and used for climate simulations (Yukimoto et al. 2011, 2012; Mizuta et al. 2012).

In the dynamical core of our global model, a semi-implicit semi-Lagrangian scheme is adopted to permit a longer time step than that determined from the Courant–Friedrichs–Lewy (CFL) condition. However, with a long time step, convection-induced compensatory subsidence in a mass-flux-type cumulus scheme occasionally exceeds the CFL condition, especially when a large number of vertical levels are used and the intervals of the levels are small. To overcome the CFL limit, a conservative and monotonic semi-Lagrangian scheme is used for transport by compensatory subsidence in the new cumulus scheme. The monotonic scheme also has the advantage of ensuring nonnegative natural material transport.

The remainder of this paper is organized as follows. The new cumulus parameterization scheme is described in detail in section 2 and a brief model description is given in section 3. The validity of the new scheme is examined in section 4. Climatology of the model using this scheme is compared with that of the model using the AS scheme in section 5. The variability of the models is shown in section 6. Computational costs of the new scheme and other schemes are estimated in section 7. Finally, a summary and conclusions are given in section 8.

2. Cumulus parameterization

The new cumulus parameterization scheme represents a spectrum of cumulus clouds by interpolating between two convective updrafts with large and small turbulent entrainment/detrainment rates. Figure 1 is a schematic diagram of the new scheme. As in Tiedtke (1989), organized entrainment occurs through the organized inflow associated with large-scale convergence, and turbulent entrainment and detrainment occur through the turbulent exchange of mass through cloud edges. Two Tiedtke-type convective updrafts, cumulus [a] and cumulus [b], are calculated layer by layer from the cloud bottom layer up to the highest cloud top layer. Cumulus [a] has the minimum entrainment/detrainment rate and the highest cloud top, while cumulus [b] has the maximum entrainment/detrainment rate at the cloud bottom. A continuous range of convective updrafts is assumed to be present with entrainment/detrainment rates between those of cumulus [a] and cumulus [b]. In-cloud variables in the convective updrafts, such as virtual temperature, dry static energy, water vapor, and turbulent entrainment/detrainment rate, are estimated by interpolating those of cumulus [a] and cumulus [b]. Where the virtual temperatures in convective updrafts with relatively larger entrainment/detrainment rates fall below the virtual temperature in the environment at some vertical level, the updrafts lose buoyancy and are detrained at that level as organized detrainment. Above this level, the convective updraft that has the largest entrainment/detrainment rate but still has positive buoyancy is considered as cumulus [b]. This calculation is repeated layer by layer until all convective updrafts lose buoyancy and are detrained as organized detrainment.

a. Convective updraft

Following Yanai et al. (1973) and Nordeng (1994), and also considering cloud ice, the steady-state equations for mass flux, dry static energy, water vapor, cloud water/ice content, and cloud ice content in the convective updraft of the cloud type (i), whose cloud top is at the vertical level i, are as follows:

$$\frac{\partial}{\partial z}M_u^{(i)} = E_u^{(i)} - D_u^{(i)}, \tag{1}$$

$$\frac{\partial}{\partial z}(M_u^{(i)}s_u^{(i)}) = E_u^{(i)}\overline{s} - D_u^{(i)}s_u^{(i)} + L\overline{\rho}c_u^{(i)} + (L_{\mathrm{subl}} - L_{\mathrm{vap}})\overline{\rho}f_u^{(i)}, \tag{2}$$

$$\frac{\partial}{\partial z}(M_u^{(i)}q_u^{(i)}) = E_u^{(i)}\overline{q} - D_u^{(i)}q_u^{(i)} - \overline{\rho}c_u^{(i)}, \tag{3}$$

$$\frac{\partial}{\partial z}(M_u^{(i)}l_u^{(i)}) = E_u^{(i)}\overline{l} - D_u^{(i)}l_u^{(i)} + \overline{\rho}c_u^{(i)} - \overline{\rho}G_{\mathrm{prec}}^{(i)}, \quad \text{and} \tag{4}$$

$$\frac{\partial}{\partial z}(M_u^{(i)}l_u^{\mathrm{ice}(i)}) = E_u^{(i)}\overline{l}^{\mathrm{ice}} - D_u^{(i)}l_u^{\mathrm{ice}(i)} + \overline{\rho}c_u^{\mathrm{ice}(i)} + \overline{\rho}f_u^{(i)} - \overline{\rho}G_{\mathrm{prec}}^{\mathrm{snow}(i)}. \tag{5}$$

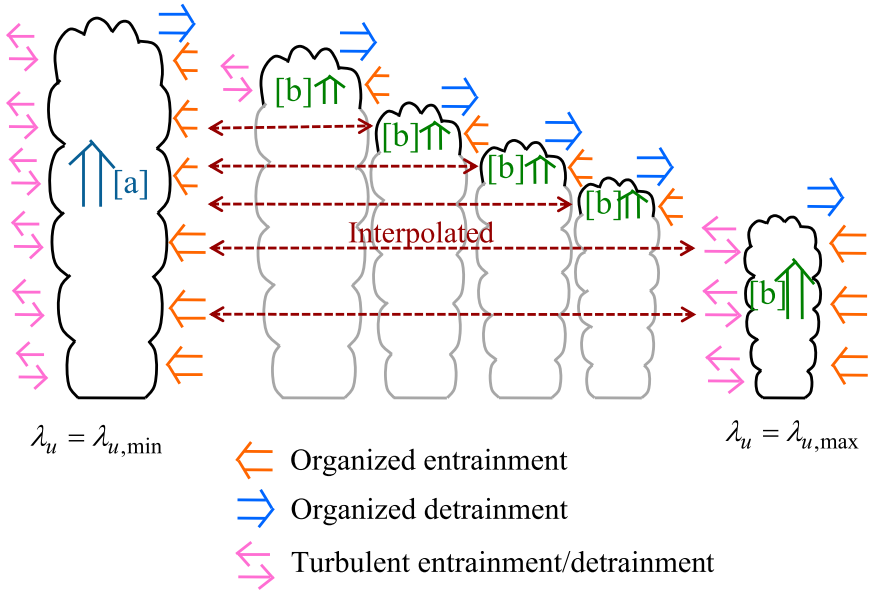

FIG. 1. Schematic diagram of the new cumulus scheme. Cumulus [a] has the minimum turbulent entrainment/detrainment rate $\lambda_{u,\min}$ and cumulus [b] has the largest turbulent entrainment/detrainment rate at each vertical level. In-cloud variables in convective updrafts with entrainment rates between those of cumulus [a] and cumulus [b] are estimated by interpolating between those of cumulus [a] and cumulus [b].

Here z is height; M_u is updraft mass flux; E_u and D_u are entrainment and detrainment rates per height, respectively; s ($\equiv c_p T + gz$) is dry static energy (T is temperature, c_p is specific heat at constant pressure, g is the gravity acceleration); q is specific humidity; l is cloud water/ice content; l^{ice} is cloud ice content; ρ is density; L_{subl} is specific latent heat of sublimation of ice; L_{vap} is specific latent heat of evaporation of water; L is specific latent heat for a water/ice mix; c_u is condensation/deposition of water vapor in the updraft; c_u^{ice} is deposition of water vapor; f_u is freezing of cloud water; G_{prec} is conversion from cloud water/ice into precipitation (rain and snow); and $G_{\text{prec}}^{\text{snow}}$ is conversion from cloud ice into snow. The subscript u (A_u) denotes the value in the updraft, and the overbar ($\overline{A}$) represents the value in the environment. The cumulus clouds are classified according to the height of the cloud top and the suffix (i) is used as the index of a classified cloud type. The values of $c_u^{\text{ice}(i)}$ and L are obtained from

$$c_u^{\text{ice}(i)} = \eta c_u^{(i)}, \qquad \text{and} \tag{6}$$

$$L = \eta L_{\text{subl}} + (1-\eta) L_{\text{vap}}, \tag{7}$$

where η is the proportion of c_u^{ice} to c_u, given here by an empirical function of $\overline{T}$: η is 1 when $\overline{T}$ is below −15°C, decreasing linearly to zero as $\overline{T}$ increases from −15° to 0°C, and zero when $\overline{T}$ is above 0°C. When the ratio of l^{ice} to l is given as a function of $\overline{T}$ (e.g., $l^{\text{ice}} = \eta l$), $f_u^{(i)}$ is determined from Eq. (5). When l^{ice} is a prognostic variable, $f_u^{(i)}$ is determined so that, for example, $l_u^{\text{ice}(i)}$ would not be less than $\eta l_u^{(i)}$.

If the upward mass fluxes of all cloud types (i) are independently calculated layer by layer using Eqs. (1)–(5), $O(N^2)$ calculations are necessary, where N is the number of the vertical levels in the troposphere. In the new cumulus scheme, only two convective updrafts, cumulus [a] with a small entrainment/detrainment rate and cumulus [b] with a large entrainment/detrainment rate, are explicitly calculated to reduce the computational cost, and the number of calculations is only $O(N)$. Comparison of roughly estimated computational time among some types of cumulus schemes is shown in section 7. In-cloud variables in convective updrafts with intermediate entrainment/detrainment rates are estimated by linear interpolation between those in cumulus [a] and cumulus [b]. Since the cumulus convection is a nonlinear phenomenon, the estimation using linear interpolation is an approximation. The validity of using linear interpolation is shown in section 4.

First, the provisional values of mass flux, entrainment, and detrainment are calculated. Second, their final values are determined by a closure assumption. Hereafter, the tilde ($\tilde{A}$) denotes provisional values.

Provisional entrainment and detrainment consist of organized and turbulent contributions:

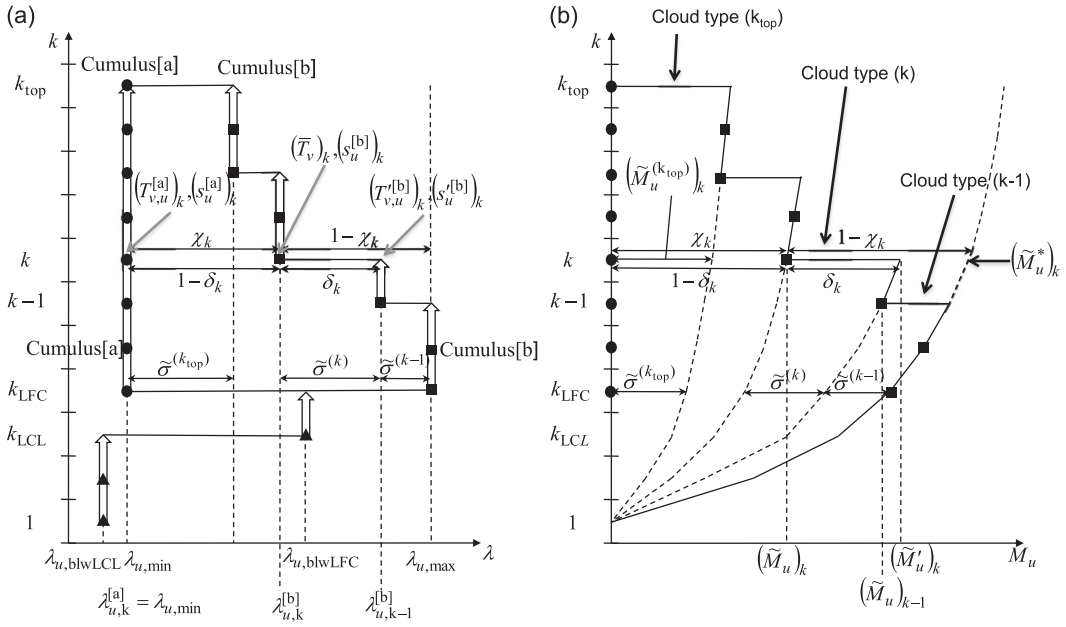

FIG. 2. Schematic diagrams of the new cumulus scheme. (a) Relations between the vertical level k and turbulent entrainment/detrainment rates λ_u. Black circles show λ_u of cumulus [a] and black squares show λ_u of cumulus [b] at each vertical level. Black triangles show λ_u below k_{LFC}. (b) Vertical distribution of the provisional upward mass flux $\tilde{M}_u$.

$$\tilde{E}_u^{[a]} = \tilde{E}_u^{org} + \tilde{E}_u^{trb[a]}, \tag{8}$$

$$\tilde{E}_u^{[b]} = \tilde{E}_u^{org} + \tilde{E}_u^{trb[b]}, \tag{9}$$

$$\tilde{D}_u^{[a]} = \tilde{D}_u^{org} + \tilde{D}_u^{trb[a]}, \quad \text{and} \tag{10}$$

$$\tilde{D}_u^{[b]} = \tilde{D}_u^{org} + \tilde{D}_u^{trb[b]}, \tag{11}$$

where the superscripts [a] and [b] ($A^{[a]}$, $B^{[b]}$) are for cumulus [a] and cumulus [b], respectively; the superscript org (A^{org}) indicates organized; and the superscript trb (A^{trb}) turbulent. Both $\tilde{E}_u^{org}$ and $\tilde{D}_u^{org}$ are common in cumulus [a] and cumulus [b].

Turbulent entrainment and turbulent detrainment are set to be equal following Tiedtke (1989), and are given by

$$\tilde{E}_u^{trb[a]} = \tilde{D}_u^{trb[a]} = \mu^{[a]}\lambda_u^{[a]}\tilde{M}_u^{[a]}, \quad \text{and} \tag{12}$$

$$\tilde{E}_u^{trb[b]} = \tilde{D}_u^{trb[b]} = \mu^{[b]}\lambda_u^{[b]}\tilde{M}_u^{[b]}, \tag{13}$$

where $\lambda_u^{[a]}$ and $\lambda_u^{[b]}$ are entrainment/detrainment rates satisfying $\lambda_u^{[a]} \le \lambda_u^{[b]}$, and $\mu^{[a]}$ and $\mu^{[b]}$ are the enhancement factors to take into account enhanced turbulence in the lower part of the cumulus [(European Centre for Medium-Range Weather Forecasts) ECMWF 2006]. The enhancement factors vary linearly from 2 at the lowest condensation level (LCL) to 1 at 1500 m above LCL. Figure 2a shows the relationship between the vertical level k and λ_u. Both $\lambda_u^{[a]}$ and $\lambda_u^{[b]}$ are set to be equal below the level k_{LFC}, where k_{LFC} is the vertical level above which lifted air becomes buoyant [level of free convection (LFC)]. At the level k_{LFC}, they are set to be $\lambda_u^{[a]} = \lambda_{u,\min}$ and $\lambda_u^{[b]} = \lambda_{u,\max}$, where $\lambda_{u,\min}$ and $\lambda_{u,\max}$ are the minimum and maximum entrainment/detrainment rates, respectively, and are given by

$$\lambda_{u,\,\min} = 0.5 \times 10^{-4}\,\mathrm{m}^{-1}, \quad \text{and} \tag{14}$$

$$\lambda_{u,\max} = 3.0 \times 10^{-4}\,\mathrm{m}^{-1}. \tag{15}$$

In Tiedtke (1989), the entrainment/detrainment rate for deep convection is $1.0 \times 10^{-4}\,\mathrm{m}^{-1}$ and that for shallow convection is $3.0 \times 10^{-4}\,\mathrm{m}^{-1}$. Above the level k_{LFC}, a spectrum of cumulus clouds is considered. When calculating the provisional mass flux, the probability density function (PDF) of cumulus clouds for entrainment/detrainment rates between $\lambda_{u,\min}$ and $\lambda_{u,\max}$ is assumed to be constant. Above the level k_{LFC}, $\lambda_u^{[a]}$ is set to the constant value $\lambda_{u,\min}$, and $\lambda_u^{[b]}$ decreases with height. In Fig. 2a, the larger λ_u, the lower the cloud top, because buoyancy is lower. The calculation of $\lambda_u^{[a]}$ and $\lambda_u^{[b]}$ is described in appendix A.

From Eqs. (8) to (13),

$$\tilde{E}_u^{[a]} - \tilde{D}_u^{[a]} = \tilde{E}_u^{[b]} - \tilde{D}_u^{[b]} = \tilde{E}_u^{org} - \tilde{D}_u^{org} \tag{16}$$

is satisfied. Therefore, $\tilde{M}_u^{[a]}$ and $\tilde{M}_u^{[b]}$ have the same value, denoted as $\tilde{M}_u$, and satisfy

$$\frac{\partial}{\partial z}\tilde{M}_u\left(=\frac{\partial}{\partial z}\tilde{M}_u^{[a]}=\frac{\partial}{\partial z}\tilde{M}_u^{[b]}\right)=\tilde{E}_u^{org}-\tilde{D}_u^{org}. \quad (17)$$

The variable $\tilde{E}_u^{org}$ consists of two kinds of organized entrainment:

$$\tilde{E}_u^{org}=\tilde{E}_u^{org1}+\tilde{E}_u^{org2}. \quad (18)$$

The variable $\tilde{E}_u^{org1}$ is the organized entrainment from the layers with high moist static energy $\overline{h}$ ($\equiv c_p\overline{T}+g\overline{z}+L\overline{q}$) and is given by

$$\tilde{E}_u^{org1}=\overline{\rho}\max[\overline{h}-(\overline{h}_{max}-\Delta h),0.0], \quad (19)$$

where $\overline{h}_{max}$ is the maximum value of $\overline{h}$ below the level of minimum saturated moist static energy and $\Delta h=2.0c_p$, the value of which is chosen empirically. Here, the vertical profile, not the magnitude, of the provisional value $\tilde{E}_u^{org1}$ is important because the magnitude of the final value E_u^{org1} is determined using a closure assumption [see Eq. (B9)]. Deep and shallow convection occur when the maximum value of $\overline{h}$ lies in the boundary layer, and midlevel convection occurs when the maximum lies in the midlevel of the troposphere. The variable $\tilde{E}_u^{org2}$ is the organized entrainment associated with the grid scale convergence $-\nabla\cdot\overline{\mathbf{v}}$ and given by

$$\tilde{E}_u^{org2}(z)=\tilde{M}_u\min[\max(A,B),C],$$

$$A=c_A\frac{\mathrm{Conv}\overline{\rho}}{\int_{z_{sfc}}^{z}(\mathrm{Conv}+\varepsilon_{Conv})\overline{\rho}\,dz},\quad c_A=0.5,$$

$$\mathrm{Conv}=\max(-\nabla\cdot\overline{\mathbf{v}},0.0),\quad \varepsilon_{Conv}=\frac{0.001}{3600},$$

$$B=c_B\frac{\overline{\rho}}{\int_{z_{sfc}}^{z}\overline{\rho}\,dz},\quad c_B=0.1,$$

$$C=c_C\frac{\overline{\rho}}{\int_{z_{sfc}}^{z}\overline{\rho}\,dz},\quad c_C=1.0, \quad (20)$$

where z_{sfc} is the surface height and the unit of Conv is s^{-1}. The variable ε_{Conv} is a small value for the denominator not to be zero. The variable B is the lower limit of A, which ensures that a small amount of organized entrainment occurs even without horizontal convergence. The variable C is the upper limit of A, and ensures that the organized entrainment is not unnaturally large. The values of ε_{Conv}, c_A, c_B, and c_C are chosen empirically. (When $c_B=c_C=1.0$, the mass flux becomes proportional to $p_{sfc}-p$, where p_{sfc} is surface pressure.) Here, the organized entrainment is determined from the mass convergence (e.g., Lindzen 1988; Kuell and Bott 2009), not from the moisture convergence (e.g., Tiedtke 1989).

The calculation of in-cloud variables such as $\tilde{M}_u$, $\lambda_u^{[b]}$, $s_u^{[a]}$, and $s_u^{[b]}$ by discretizing Eqs. (1)–(20) is shown in appendix A.

b. Closure assumption

The final value of a mass flux of each cloud type is determined from the provisional value by using a closure assumption.

Figure 2b shows the vertical distribution of the provisional upward mass flux $\tilde{M}_u$. As shown in Fig. 2b, $\tilde{M}_u$ can be divided into the mass fluxes of multiple cloud types, $\tilde{M}_u^{(i)}$, where i denotes the vertical level of the cloud top. The proportion of the provisional mass flux of the cloud type (i), $\tilde{\sigma}^{(i)}$, at the vertical level $k=k_{LFC}$ is

$$\tilde{\sigma}^{(i)}=\frac{(\tilde{M}_u^{(i)})_{k_{LFC}}}{(\tilde{M}_u)_{k_{LFC}}}\quad\left(\sum_i\tilde{\sigma}^{(i)}=1\right). \quad (21)$$

The mass flux of the cloud type (i), $M_u^{(i)}$, is determined from

$$M_u^{(i)}=\alpha^{(i)}\tilde{M}_u^{(i)}. \quad (22)$$

The value of $\alpha^{(i)}$ is calculated from the closure assumption. The closure assumption used here is based on convective available potential energy (CAPE; Fritsch and Chappell 1980; Nordeng 1994; ECMWF 2006). CAPE is given by

$$\mathrm{CAPE}=\int_{cloud}\left[\frac{g}{\overline{T}_v}(T_{v,u}-\overline{T}_v)\right]dz, \quad (23)$$

where $T_v\equiv T(1+0.608q)+l$ is the virtual temperature. It is assumed that an ensemble of convections has the effect of decreasing CAPE over a relaxation time τ, and the convection of the cloud type (i) works to decrease $\mathrm{CAPE}^{(i)}\tilde{\sigma}^{(i)}$ over the relaxation time, where $\mathrm{CAPE}^{(i)}$ is the CAPE of the cloud type (i). By this assumption,

$$\left(\frac{\partial\mathrm{CAPE}}{\partial t}\right)^{(i)}=-\frac{\mathrm{CAPE}^{(i)}\tilde{\sigma}^{(i)}}{\tau}\quad\left(\tau=3600\frac{160}{N+1}\right) \quad (24)$$

is obtained, where $(\partial\mathrm{CAPE}/\partial t)^{(i)}$ is the decrease of $\mathrm{CAPE}^{(i)}$ per unit time due to the convection of the cloud type (i), and N is the truncation wavenumber of the spectral model. The variable τ is made dependent on model resolution as in ECMWF (2006). In the actual

calculation, not only CAPE but also convective inhibition (CIN) is considered. CIN is obtained from

$$\mathrm{CIN} = \int_{\mathrm{below\_cloud}} \left[\frac{g}{\overline{T}_v} (\overline{T}_v - T_{v,u}) \right] dz. \tag{25}$$

Here, below_cloud means below the level k_{LFC}, where $\overline{T}_v - T_{v,u} > 0$ is satisfied. When determining the value of $\alpha^{(i)}$ in Eq. (22), we use

$$\left(\frac{\partial \mathrm{CAPE}}{\partial t} \right)^{(i)} = -\frac{\max(\mathrm{CAPE}^{(i)} - \mathrm{CIN}, 0.3\mathrm{CAPE}^{(i)})\tilde{\sigma}^{(i)}}{\tau} \tag{26}$$

instead of Eq. (24) so that the mass fluxes of convective updrafts become smaller when CIN is large. Appendix B shows how to calculate $\alpha^{(i)}$ diagnostically from Eq. (26) and how to obtain the final values of mass flux, entrainment, and detrainment from their provisional values.

Here, τ is independent of cloud type (i), but τ can depend on cloud type. For example, τ can be larger in the convection whose cloud top is lower, which weakens shallow convections. Moreover, different closure assumption can be used dependent on the cumulus height. For example, non-CAPE-type closure assumption (e.g., Tiedtke 1989; Park and Bretherton 2009) can be used in shallow convection.

c. Convective downdraft

Only a single mass flux for the convective downdraft is calculated for simplicity. The convective downdraft is calculated using the following equations:

$$\begin{aligned} \frac{\partial}{\partial z} M_d &= E_d - D_d \\ &= (E_d^{\mathrm{org}} + E_d^{\mathrm{trb}}) - (D_d^{\mathrm{org}} + D_d^{\mathrm{trb}}), \end{aligned} \tag{27}$$

$$\begin{aligned} \frac{\partial}{\partial z}(M_d s_d) = {} & E_d^{\mathrm{org}} s_{\mathrm{mix}} + E_d^{\mathrm{trb}} \overline{s} - (D_d^{\mathrm{org}} + D_d^{\mathrm{trb}}) s_d \\ & - L\overline{\rho}(e_d^{\mathrm{cld}} + e_d^{\mathrm{prec}}), \end{aligned} \tag{28}$$

$$\begin{aligned} \frac{\partial}{\partial z}(M_d q_d) = {} & E_d^{\mathrm{org}} q_{\mathrm{mix}} + E_d^{\mathrm{trb}} \overline{q} - (D_d^{\mathrm{org}} + D_d^{\mathrm{trb}}) q_d \\ & + \overline{\rho}(e_d^{\mathrm{cld}} + e_d^{\mathrm{prec}}), \end{aligned} \tag{29}$$

$$\begin{aligned} \frac{\partial}{\partial z}(M_d l_d) = {} & E_d^{\mathrm{org}} l_{\mathrm{mix}} + E_d^{\mathrm{trb}} \overline{l} - (D_d^{\mathrm{org}} + D_d^{\mathrm{trb}}) l_d \\ & - \overline{\rho}(e_d^{\mathrm{cld}}), \quad l_d = 0, \end{aligned} \tag{30}$$

$$\begin{aligned} \frac{\partial}{\partial z}(M_d l_d^{\mathrm{ice}}) = {} & E_d^{\mathrm{org}} l_{\mathrm{mix}}^{\mathrm{ice}} + E_d^{\mathrm{trb}} \overline{l}^{\mathrm{ice}} - (D_d^{\mathrm{org}} + D_d^{\mathrm{trb}}) l_d^{\mathrm{ice}} \\ & - \overline{\rho}(e_d^{\mathrm{cldice}}), \quad l_d^{\mathrm{ice}} = 0, \quad \text{and} \end{aligned} \tag{31}$$

$$e_d^{\mathrm{cldice}} + e_d^{\mathrm{snow}} = \eta(e_d^{\mathrm{cld}} + e_d^{\mathrm{prec}}), \tag{32}$$

where $M_d(<0)$ is the downdraft mass flux; E_d and D_d are entrainment and detrainment rates, respectively; and e_d^{cld}, e_d^{cldice}, e_d^{prec}, and e_d^{snow} are evaporation of cloud water/ice, evaporation (sublimation) of cloud ice, precipitation (rain/snow), and snow in the downdraft, respectively. The subscript d (A_d) denotes the value in the downdraft, and the subscript mix (A_{mix}) denotes the value in the equal mixture of detrainment from updrafts and environmental air. Half of the detrainment from the updrafts, $D_u/2$ (but with the upper limit of D_u^{trb}), is supposed to be equally mixed with the environmental air cooled to the wet-bulb temperature and saturated by evaporation of precipitation. When the mixture has negative buoyancy below the level of the minimum saturated moist static energy, it becomes the organized entrainment into the downdraft E_d^{org}. The variable E_d^{org} has an upper limit so that M_d does not exceed $0.3M_u$. The organized entrainment at multiple vertical levels is taken into consideration unlike in Tiedtke (1989). The turbulent entrainment and detrainment have the same value and satisfy the following equations (Tiedtke 1989):

$$E_d^{\mathrm{trb}} = D_d^{\mathrm{trb}} = \lambda_d(-M_d), \quad \text{and} \tag{33}$$

$$\lambda_d = 2.0 \times 10^{-4}\ \mathrm{m}^{-1}. \tag{34}$$

The air in the downdraft is saturated by the evaporation of precipitation and cloud water. When the downdraft becomes positively buoyant at a specific level, the entire downdraft mass flux detrains at that level as organized detrainment. Otherwise, the organized detrainment from the downdraft occurs within the subcloud layer.

The method used to discretize Eqs. (27)–(29) is shown in appendix C.

d. Precipitation and convective momentum transport

The conversion from cloud water to precipitation in Eq. (4) is calculated from the Sundqvist (1978) type equation. Melting of falling snow is assumed to occur at a few vertical levels near 0°C.

The vertical transports of horizontal momentum by the convective updrafts and the convective downdraft are also calculated, where pressure gradient force related to the environmental wind shear (Wu and Yanai 1994; Gregory et al. 1997) is taken into consideration.

e. Feedback to the environment

The time evolution of the variables in the environment due to the cumulus scheme is given by the following equations:

$$\left(\frac{\partial \overline{s}}{\partial t}\right)_{\mathrm{cu}} = \sum_i \left[-\frac{1}{\overline{\rho}}\frac{\partial}{\partial z}(M_u^{(i)} s_u^{(i)} - M_u^{(i)}\overline{s}) + L c_u^{(i)} + (L_{\mathrm{subl}} - L_{\mathrm{vap}}) f_u^{(i)}\right] - \frac{1}{\overline{\rho}}\frac{\partial}{\partial z}(M_d s_d - M_d \overline{s}) - L(e_d^{\mathrm{cld}} + e_d^{\mathrm{prec}}) - L_{\mathrm{vap}} e_{\mathrm{prec}} - (L_{\mathrm{subl}} - L_{\mathrm{vap}})(e_{\mathrm{prec}}^{\mathrm{snow}} + m_{\mathrm{prec}} - f_{\mathrm{prec}} + m_{\mathrm{cldice}}), \tag{35}$$

$$\left(\frac{\partial \overline{q}}{\partial t}\right)_{\mathrm{cu}} = \sum_i \left[-\frac{1}{\overline{\rho}}\frac{\partial}{\partial z}(M_u^{(i)} q_u^{(i)} - M_u^{(i)}\overline{q}) - c_u^{(i)}\right] - \frac{1}{\overline{\rho}}\frac{\partial}{\partial z}(M_d q_d - M_d \overline{q}) + e_d^{\mathrm{cld}} + e_d^{\mathrm{prec}} + e_{\mathrm{prec}}, \tag{36}$$

$$\left(\frac{\partial \overline{l}}{\partial t}\right)_{\mathrm{cu}} = \sum_i \left[-\frac{1}{\overline{\rho}}\frac{\partial}{\partial z}(M_u^{(i)} l_u^{(i)} - M_u^{(i)}\overline{l}) + c_u^{(i)} - G_p^{(i)}\right] - \frac{1}{\overline{\rho}}\frac{\partial}{\partial z}(M_d l_d - M_d \overline{l}) - e_d^{\mathrm{cld}}, \quad \text{and} \tag{37}$$

$$\left(\frac{\partial \overline{l}^{\mathrm{ice}}}{\partial t}\right)_{\mathrm{cu}} = \sum_i \left[-\frac{1}{\overline{\rho}}\frac{\partial}{\partial z}(M_u^{(i)} l_u^{\mathrm{ice}(i)} - M_u^{(i)}\overline{l}^{\mathrm{ice}}) + c_u^{\mathrm{ice}(i)} + f_u^{(i)} - G_p^{\mathrm{snow}(i)}\right] - \frac{1}{\overline{\rho}}\frac{\partial}{\partial z}[M_d l_d^{\mathrm{ice}} - M_d \overline{l}^{\mathrm{ice}}] - e_d^{\mathrm{cldice}} + m_{\mathrm{cldice}}, \tag{38}$$

where m_{cldice} is melting of cloud ice along with the compensatory subsidence. Using Eqs. (2)–(5) and Eqs. (28)–(31), Eqs. (35)–(38) can be rewritten as follows:

$$\left(\frac{\partial \overline{s}}{\partial t}\right)_{\mathrm{cu}} = \frac{1}{\overline{\rho}}\frac{\partial}{\partial z}[(M_u + M_d)\overline{s}] + \frac{1}{\overline{\rho}}\left[-\left\{\sum_i (E_u^{(i)})\right\}\overline{s} + \left\{\sum_i (D_u^{(i)} s_u^{(i)})\right\} - E_d^{\mathrm{org}} s_{\mathrm{mix}} - E_d^{\mathrm{trb}}\overline{s} + (D_d^{\mathrm{org}} + D_d^{\mathrm{trb}}) s_d\right] - L_{\mathrm{vap}} e_{\mathrm{prec}} - (L_{\mathrm{subl}} - L_{\mathrm{vap}})(e_{\mathrm{prec}}^{\mathrm{snow}} + m_{\mathrm{prec}} - f_{\mathrm{prec}} + m_{\mathrm{cldice}}), \tag{39}$$

$$\left(\frac{\partial \overline{q}}{\partial t}\right)_{\mathrm{cu}} = \frac{1}{\overline{\rho}}\frac{\partial}{\partial z}[(M_u + M_d)\overline{q}] + \frac{1}{\overline{\rho}}\left[-\left\{\sum_i (E_u^{(i)})\right\}\overline{q} + \left\{\sum_i (D_u^{(i)} q_u^{(i)})\right\} - E_d^{\mathrm{org}} q_{\mathrm{mix}} - E_d^{\mathrm{trb}}\overline{q} + (D_d^{\mathrm{org}} + D_d^{\mathrm{trb}}) q_d\right] + e_{\mathrm{prec}}, \tag{40}$$

$$\left(\frac{\partial \overline{l}}{\partial t}\right)_{\mathrm{cu}} = \frac{1}{\overline{\rho}}\frac{\partial}{\partial z}[(M_u + M_d)\overline{l}] + \frac{1}{\overline{\rho}}\left[-\left\{\sum_i (E_u^{(i)})\right\}\overline{l} + \left\{\sum_i (D_u^{(i)} l_u^{(i)})\right\} - E_d^{\mathrm{org}} l_{\mathrm{mix}} - E_d^{\mathrm{trb}}\overline{l}\right], \quad \text{and} \tag{41}$$

$$\left(\frac{\partial \overline{l}^{\mathrm{ice}}}{\partial t}\right)_{\mathrm{cu}} = \frac{1}{\overline{\rho}}\frac{\partial}{\partial z}[(M_u + M_d)\overline{l}^{\mathrm{ice}}] + \frac{1}{\overline{\rho}}\left[-\left\{\sum_i (E_u^{(i)})\right\}\overline{l}^{\mathrm{ice}} + \left\{\sum_i (D_u^{(i)} l_u^{\mathrm{ice}(i)})\right\} - E_d^{\mathrm{org}} l_{\mathrm{mix}}^{\mathrm{ice}} - E_d^{\mathrm{trb}}\overline{l}^{\mathrm{ice}}\right] + m_{\mathrm{cldice}}. \tag{42}$$

The method used to discretize Eq. (39) is shown in appendix D.

f. Compensatory subsidence

The first terms on the right-hand side of Eqs. (39)–(42) show downward transport accompanying compensatory subsidence. To calculate the downward transport, we adopt a conservative and monotonic one-dimensional flux-form semi-Lagrangian scheme (Lin and Rood 1996), where we use the piecewise rational method (PRM; Xiao and Peng 2004) for the vertical monotonic interpolation of variables in the environment. PRM is more accurate and less diffusive than the piecewise linear method. Using the monotonic semi-Lagrangian scheme ensures nonnegative and nonoscillatory natural transport of materials such as cloud water, cloud ice, and aerosols. The calculation of transport using the semi-Lagrangian scheme is shown in appendix E. This useful scheme is also employed in the calculation of vertical flux in the dynamical core of our global model (the vertically conservative semi-Lagrangian scheme; Yoshimura and Matsumura 2003, 2005; Yukimoto et al. 2011) and in the vertical grid transformation in the general-purpose coupler Scup (Yoshimura and Yukimoto 2008).

In the AS scheme in our model, the transport by compensatory subsidence is calculated with an explicit Eulerian scheme. Therefore, the mass-flux limiter is used to satisfy the CFL condition, but the limiter has a bad

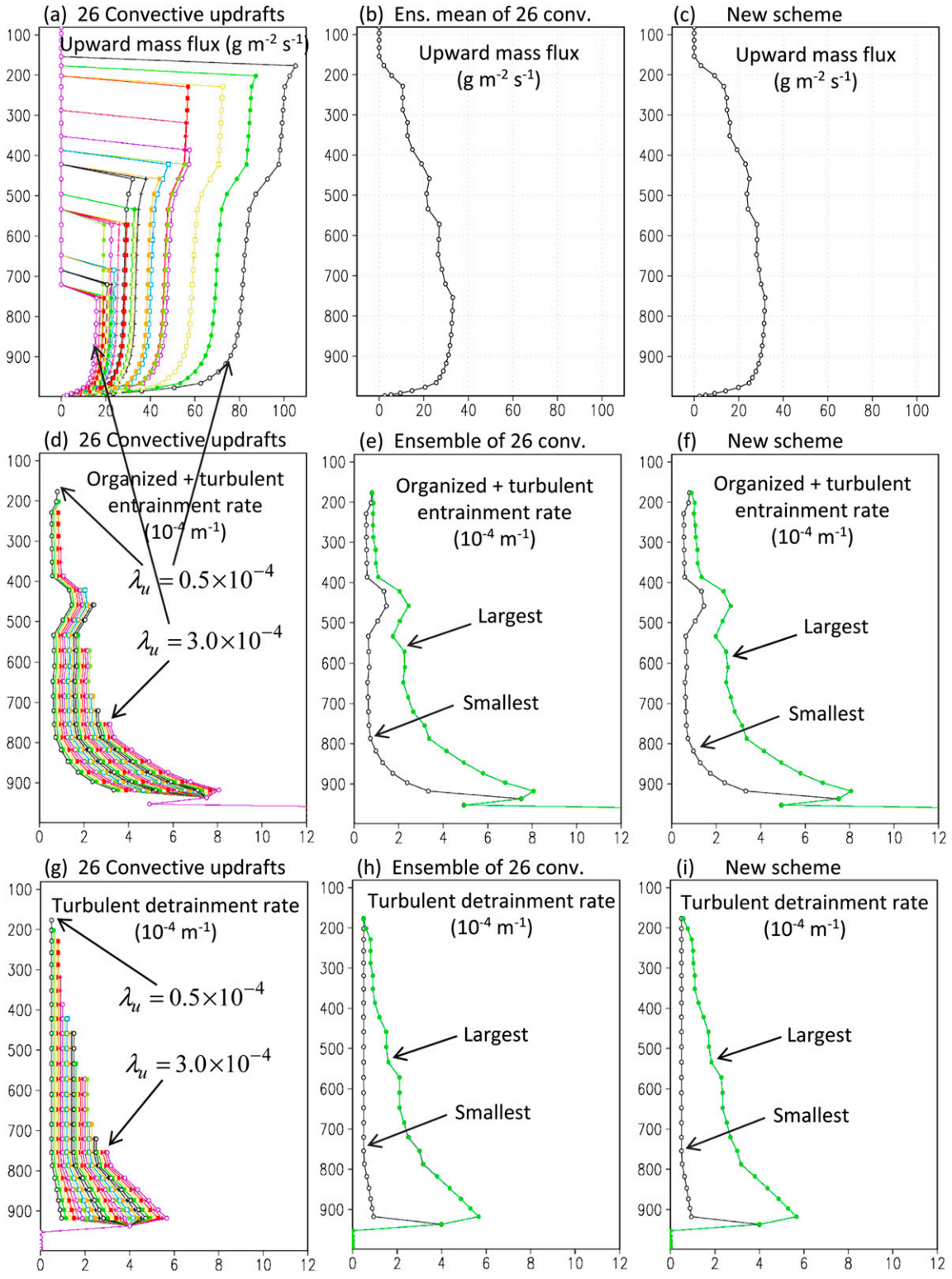

FIG. 3. Vertical profiles of (a)–(c) the mass fluxes, (d)–(f) the organized plus turbulent entrainment rates, and (g)–(i) the turbulent detrainment rates. (a),(d),(g) The 26 ensemble members, each of which has the different entrainment/detrainment rate $\lambda_u = 0.5 \times 10^{-4} + 0.1 \times 10^{-4}(j-1)$, where $j = 1, 2, \ldots,$ or 26 (i.e., $0.5 \times 10^{-4}, 0.6 \times 10^{-4}, \ldots,$ or 3.0×10^{-4}). (b) Ensemble mean of the mass fluxes of the 26 members. (e),(h) The largest and the smallest values of entrainment and detrainment rates of the ensemble members. (c),(f),(i) Results of the new scheme with $\lambda_{u,\min} = 0.5 \times 10^{-4}$ and $\lambda_{u,\max} = 3.0 \times 10^{-4}$.

influence on model results (Lopez and Moreau 2005; ECMWF 2006) especially when a large time step is used and the intervals of the vertical levels are small. A semi-implicit scheme can be used to relax the CFL condition, but the implicit solution provides smoother and nonlocal vertical profiles of tendencies through its inherent diffusivity (ECMWF 2006). The semi-Lagrangian scheme described here relaxes the CFL condition and provides less diffusive profiles.

3. Model description

We use the Meteorological Research Institute atmospheric general circulation model (MRI-AGCM v3.2; Mizuta et al. 2012), which is based on the model jointly developed by the Japan Meteorological Agency (JMA) and the MRI (Mizuta et al. 2006). In MRI-AGCM v3.2, a two-time-level semi-implicit semi-Lagrangian scheme is used for time integration to allow a long time step. A vertically conservative semi-Lagrangian scheme (see section 2f) is adopted, and a correction method similar to that described by Priestley (1993) and by Gravel and Staniforth (1994) is used horizontally for global conservation of tracers. Some new physical parameterization schemes have been introduced as options into the model to make it more suitable for long-term simulations such as global warming experiments. The cumulus scheme options are the AS scheme used in the JMA operational model (Arakawa and Schubert 1974; Moorthi and Suarez 1992; Pan and Randall 1998; JMA 2007), the Kain–Fritsch scheme, and the new cumulus scheme described here. The cloud scheme options are the Smith scheme (Smith 1990) used in the JMA operational model, the Tiedtke scheme (Tiedtke 1993; Kawai 2006), and a two-moment bulk scheme newly developed especially for the MRI Earth System Model (Yukimoto et al. 2011). In this paper, we compare model simulations with the AS cumulus scheme and with the new cumulus scheme, using the Tiedtke cloud scheme in both cases.

4. Validity of the new cumulus scheme interpolating between two convective updrafts

To validate the new cumulus scheme, we compare results using the new cumulus scheme with those from an ensemble of runs of a Tiedtke-type scheme (a bulk mass-flux scheme with one convective updraft) using different entrainment rates. Each run of the Tiedtke-type scheme is performed by letting $\lambda_{u,\min} = \lambda_{u,\max}$ in the new cumulus scheme. We use the results of one time step runs on 1 July of the third year of the 7-yr run described in section 5. (In Figs. 3–5, we show the results at the grid point 9.828°N, 137.812°E, where there are convective updrafts with different heights due to different entrainment rates.)

Figure 3 shows the vertical distribution of the upward mass fluxes of the convective updrafts (see appendix F for the calculation of the mass flux), the organized plus turbulent entrainment rates, and the turbulent detrainment rates. Figures 3a, 3d, and 3g show the results of 26 ensemble members, each of which has the different turbulent entrainment/detrainment rate $\lambda = 0.5 \times 10^{-4} + 0.1 \times 10^{-4}(j-1)\,\mathrm{m}^{-1}$, where $j = 1, 2, \ldots,$ or 26 (i.e. 0.5×10^{-4}, 0.6×10^{-4}, … , or 3.0×10^{-4}). Here the results for $\lambda = 0.6 \times 10^{-4}$, for example, are obtained by putting $\lambda_{u,\min} = \lambda_{u,\max} = 0.6 \times 10^{-4}$. The ensemble mean of the upward mass flux (Fig. 3a) is shown in Fig. 3b, which is calculated from

$$\mathrm{Mean}(a_j) = \frac{0.5a_1 + a_2 + a_3 + \cdots + a_{J-1} + 0.5a_J}{J-1}, \qquad (43)$$

where a_j is the value of each member, J is the number of members, and the weights of a_1 and a_J (corresponding to $\lambda = 0.5 \times 10^{-4}$ and $\lambda = 3.0 \times 10^{-4}$, respectively) are set to 0.5. Figures 3e and 3h show the largest and smallest values of the ensemble members at each levels for the entrainment rates (Fig. 3d) and the detrainment rates (Fig. 3g). Figures 3c, 3f, and 3i show the results of the new cumulus scheme with $\lambda_{u,\min} = 0.5 \times 10^{-4}$ and $\lambda_{u,\max} = 3.0 \times 10^{-4}$. In Figs. 3d–i, turbulent entrainment and turbulent detrainment are enhanced near the cloud bottom [$\mu^{[a]}$ and $\mu^{[b]}$ in Eqs. (12) and (13)]. In Figs. 3d–f, organized entrainment is large at lower levels and at about 400–500 hPa. The results in Figs. 3b and 3c, Figs. 3e and 3f, and Figs. 3h and 3i are very similar, indicating that the new cumulus scheme can represent the effect of the ensemble of multiple convective updrafts with different entrainment rates.

However, the upward mass flux of the new cumulus scheme in Fig. 3c is slightly larger in the upper troposphere and slightly smaller in the lower troposphere than that of the ensemble mean in Fig. 3b, and the largest entrainment rate and detrainment rate in Figs. 3f and 3i are slightly larger at the upper levels than those in Figs. 3e and 3h, which indicates that the cloud tops of convective updrafts in the new cumulus scheme are slightly higher than those in the ensemble mean.

This can be explained by Fig. 4, which shows the differences in the in-cloud virtual temperatures between the 26 members and the member with the smallest entrainment rate $\lambda_{u,\min}$. The straight line at each vertical level is the linear interpolation between the value with the smallest entrainment rate and that with the largest entrainment rate. The values of the in-cloud virtual temperature obtained by the linear interpolation are

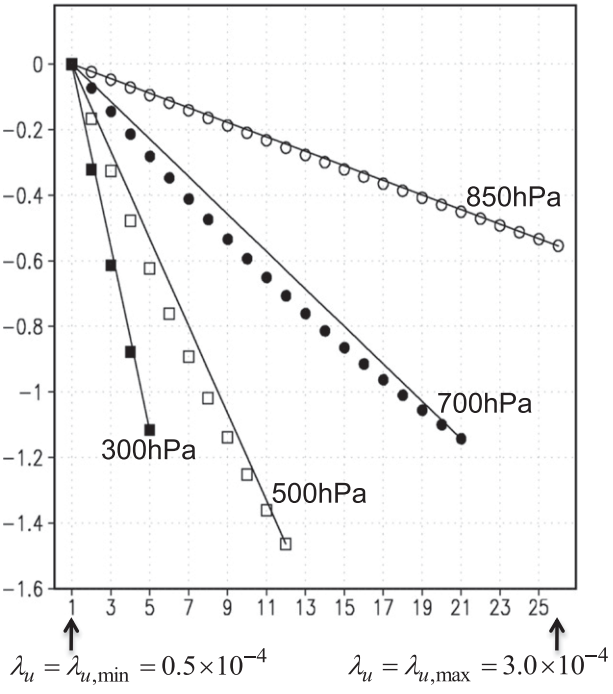

FIG. 4. Differences in in-cloud virtual temperature (K) between 26 ensemble members with different entrainment rates and the member with the smallest entrainment rate $\lambda_{u,\min}$ at the vertical levels of 300, 500, 700, and 850 hPa. The straight line at each vertical level is the linear interpolation between the value with the smallest entrainment rate (the first member) and that with the largest entrainment rate (e.g., the 21st member at the 700-hPa level).

close enough to those of the ensemble members, meaning that the linear interpolation is a good approximation. However the values of the linear interpolation are slightly larger than those of the ensemble members. That is, the virtual temperature obtained by the linear interpolation in the new cumulus scheme is slightly higher than that obtained by explicit calculation of the convective updraft with each entrainment rate. Therefore, the cloud tops of convective updrafts in the new cumulus scheme become slightly higher than those in the ensemble mean.

Figures 5a–d show the vertical distributions of the mass flux, the convective heating rate, the convective moistening rate, and the detrainment of cloud water, respectively. The results of the new cumulus scheme are compared with those of the ensemble means of 26 members, 6 members, and 2 members with equally spaced different entrainment rates. Here we suppose that an ensemble mean of an infinite number of members gives the right answer. There are 36 vertical levels below 100 hPa in the model used here, so the ensemble mean of 26 members is considered to be close enough to the right answer. The results of the new cumulus scheme are similar to those of the ensemble mean of 26 members in Figs. 5a–d. The differences are that the absolute values in the lower troposphere are slightly smaller and those in the upper troposphere are slightly larger in the new cumulus scheme compared with the ensemble mean of 26 members. This is because the cloud tops of convective updrafts in the new cumulus scheme are slightly higher than those in the ensemble mean of 26 members, as described above. The results of the ensemble mean of 2 members are very different from those of 26 members. The results of 6 members are similar to those of 26 members in Figs. 5b and 5c. However, the detrainment of the cloud water for six members (Fig. 5d) is too large at some vertical levels, indicating that an ensemble of six members is not sufficient to correctly evaluate the detrainment of cloud water.

5. Model climatology

Here we present the results of 7-yr simulations of the 60-km mesh (TL319L64) models using the AS scheme and the new cumulus scheme, and compare them with the observations. Climatological sea surface temperature (SST) and sea ice concentration of Reynolds and Smith (1994) are used as lower boundary conditions. The other boundary conditions are the same as those in the Atmospheric Model Intercomparison Project (AMIP)-type simulations presented in Mizuta et al. (2012), Murakami et al. (2012a,b), and Endo et al. (2012). In the AMIP-type simulations using the new cumulus scheme at the resolutions from TL95 (180 km) to TL959 (20 km), the resolution dependence of the results in the global-scale climate is small (Mizuta et al. 2012). In the AMIP-type simulations using the AS scheme, the maximum detrainment of cloud water content, which is used as a tunable parameter in the AS scheme, is increased to enhance precipitation in the western Pacific. Although the climatology of precipitation is improved by this tuning, a large warm bias in the tropical upper troposphere and a large wet bias in the tropical middle and upper troposphere appear. Therefore, this tuning is not used in the simulation using the AS scheme shown here.

Figures 6a and 6b show the annual mean precipitation climatology for the 7-yr simulations and the difference from the Climate Prediction Center (CPC) Merged Analysis of Precipitation (CMAP; Xie and Arkin 1997) climatology. The statistics of bias, root-mean-square error (RMSE), and correlations (CORR) are better in the new scheme simulation than in the AS scheme simulation. Scores of the precipitation climatology in Asia including the Taylor diagram (Taylor 2001) are shown in Endo et al. (2012), and Taylor diagrams for precipitation, wind/height fields, and radiation climatology are shown in Mizuta et al. (2012), where the model using the new cumulus scheme obtains good results compared with other

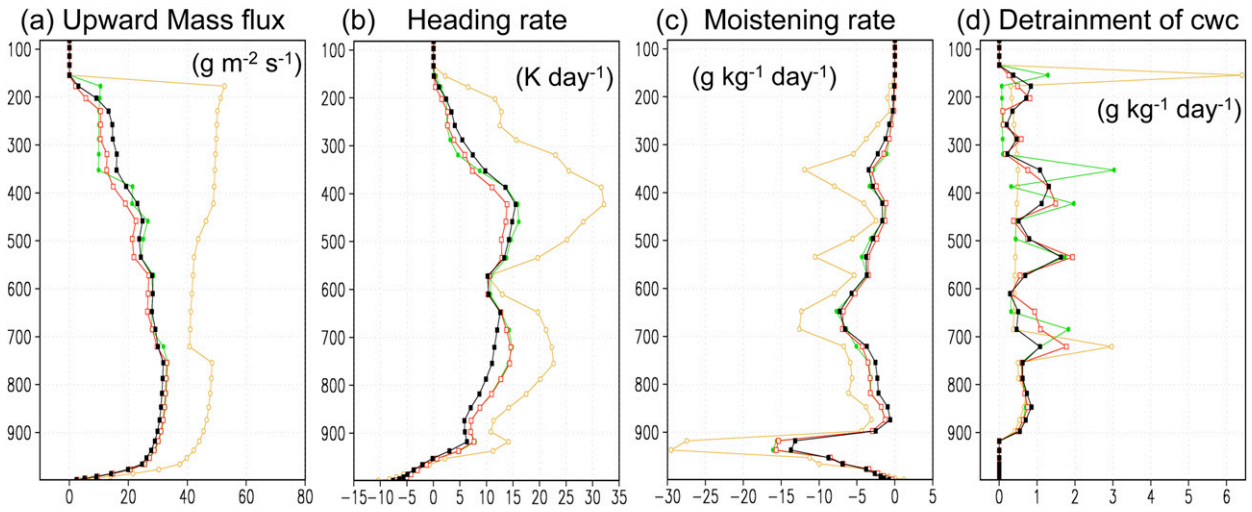

FIG. 5. Comparison of (a) the upward mass flux ($g\,m^{-2}\,s^{-1}$), (b) the heating rate ($K\,day^{-1}$), (c) the moistening rate ($g\,kg^{-1}\,day^{-1}$), and (d) the detrainment of cloud water content ($g\,kg^{-1}\,day^{-1}$) between the ensemble means of convective updrafts and the new cumulus scheme. The red line is the ensemble mean of 26 convective updrafts, each of which has the entrainment/detrainment rate 0.5×10^{-4}, 0.6×10^{-4}, . . . , or 3.0×10^{-4}. The green line is the ensemble mean of six convective updrafts, each of which has the entrainment rate 0.5×10^{-4}, 1.0×10^{-4}, . . . , or 3.0×10^{-4}. The orange line is the ensemble mean of two convective updrafts, each of which has the entrainment rate 0.5×10^{-4} or 3.0×10^{-4}. The black line is the new scheme with the minimum entrainment rate 0.5×10^{-4} and the maximum entrainment rate 3.0×10^{-4}.

models. Figure 6c shows convective precipitation, and Fig. 6d shows large-scale condensation precipitation for the simulations. The difference between the AS scheme and the new cumulus scheme simulations is large in the tropics, where there is almost no large-scale condensation precipitation in the AS scheme simulation, whereas there is some in the new cumulus scheme simulation.

Figure 7 shows the annual-mean climatology of outgoing longwave radiation (OLR) and outgoing shortwave radiation (OSR) at the top of the atmosphere. The model results are compared with the Clouds and the Earth's Radiant Energy System (CERES) Energy Balanced and Filled (EBAF) satellite dataset (Loeb et al. 2009). In the new scheme simulation, negative OLR bias and positive OSR bias appear around deep convection region in the tropics such as the intertropical convergence zone (ITCZ), while the bias is reversed in the AS scheme simulation. It has been verified that the positive OSR bias in the new scheme can be decreased by introducing the practical independent column approximation (PICA; Collins 2001; Nagasawa 2012), which improves the treatment of cloud overlap in shortwave radiation calculation. In the shallow convection regions in the subtropics, negative OLR bias and positive OSR bias are found in the AS scheme simulation. These are reduced in the new scheme, although negative OSR bias is enhanced along the west coast of the continents. It has also been verified that the negative OSR bias around these regions, as well as that in the Southern Ocean, can be reduced by including an estimation of inversion strength (EIS) by Wood and Bretherton (2006) into the stratocumulus scheme and modifying it to include the effect of cloud-top entrainment (CTE) instability (Kawai 2013).

Figure 8 shows the differences in zonal mean annual mean temperature and zonal mean specific humidity between the 7-yr simulations and the Japanese 25-year Reanalysis Project (JRA-25; Onogi et al. 2007). The warm bias in the tropical upper troposphere and the positive bias of water vapor in the tropical middle troposphere are smaller in the new cumulus scheme simulation than in the AS scheme simulation. The negative bias of water vapor at about 800–900 hPa in the subtropics is larger in the new cumulus scheme simulation. It has been verified that this bias can be decreased by weakening shallow convection. The shallow convection has the effect of drying at the low levels.

Figure 9a shows the simulated zonal mean annual mean convective updraft mass flux. The mass flux in the new cumulus scheme is larger in the lower troposphere and smaller in the upper troposphere than in the AS scheme, showing that there is more shallow/congestus convection and less penetrative convection in the new cumulus scheme than in the AS scheme. One of the reasons that there is more penetrative convection in the AS scheme is as follows: in the AS scheme in our model, the values of in-cloud variables at the cloud top are directly calculated from those at the cloud bottom without calculating conversion from cloud water/ice into precipitation at intermediate vertical levels, so freezing of cloud water is overestimated and the temperatures in the updrafts are

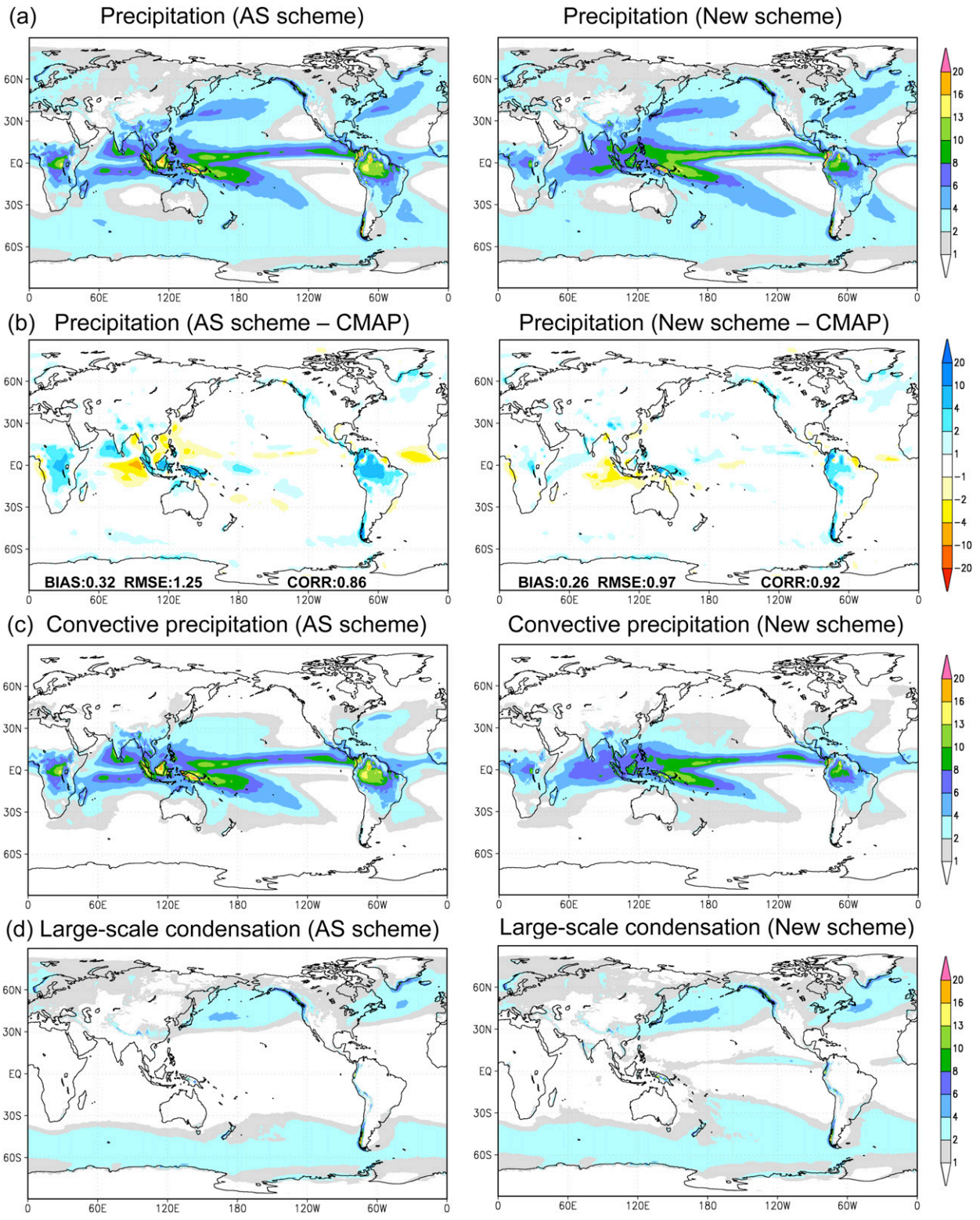

FIG. 6. Annual mean climatology of 7-yr runs of the model using (left) the AS scheme and (right) the new scheme. (a) Precipitation (mm day^{-1}), (b) difference in precipitation between the models and CMAP (mm day^{-1}), (c) convective precipitation (mm day^{-1}), and (d) large-scale condensation precipitation (mm day^{-1}). In (b), statistics of bias, root-mean-square error (RMSE), and correlation (CORR) are also shown.

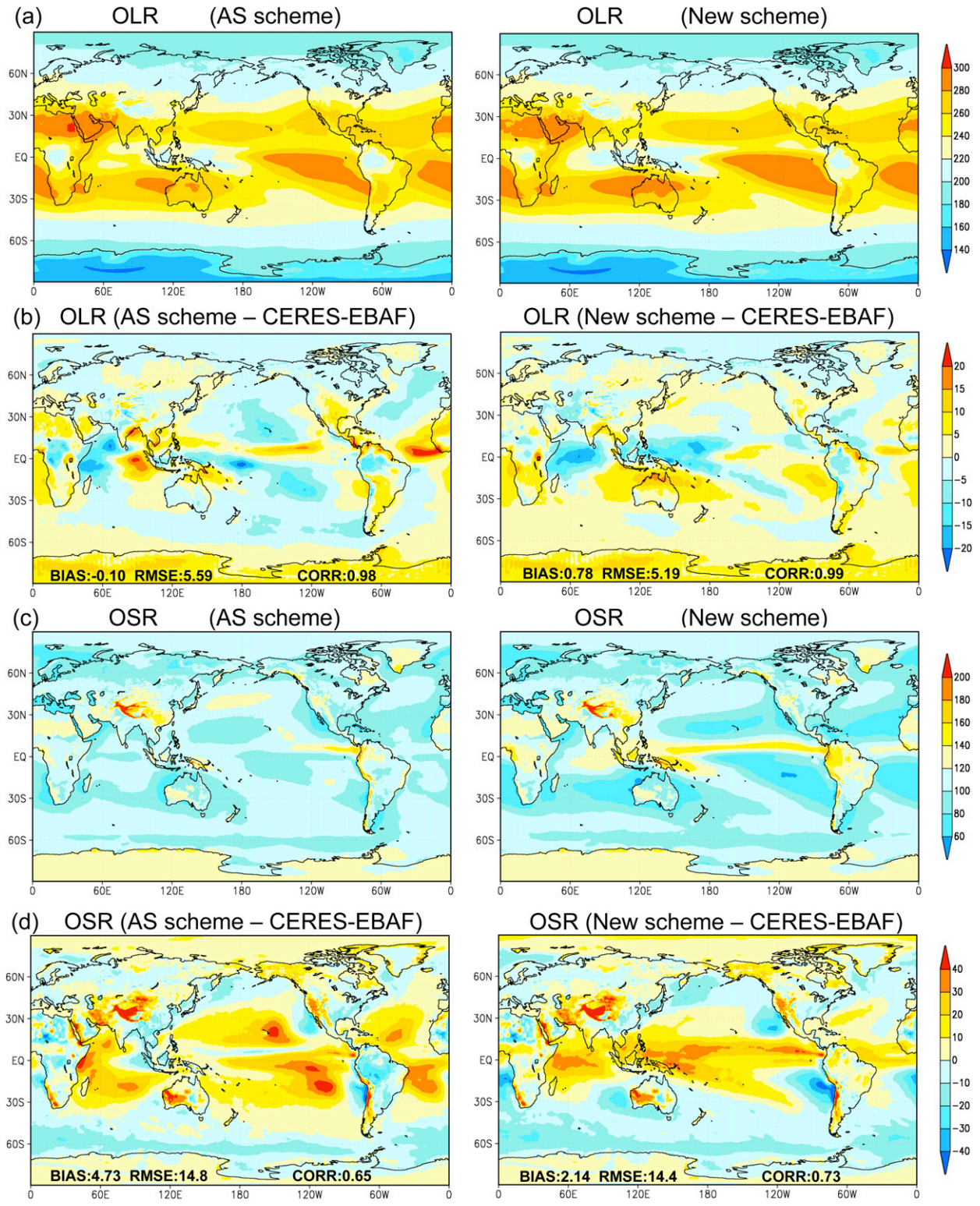

FIG. 7. As in Fig. 6, but for (a) outgoing longwave radiation (OLR), (b) difference in OLR between the models and the CERES-EBAF observation, (c) outgoing shortwave radiation (OSR), and (d) difference in OSR between the models and the CERES EBAF observation.

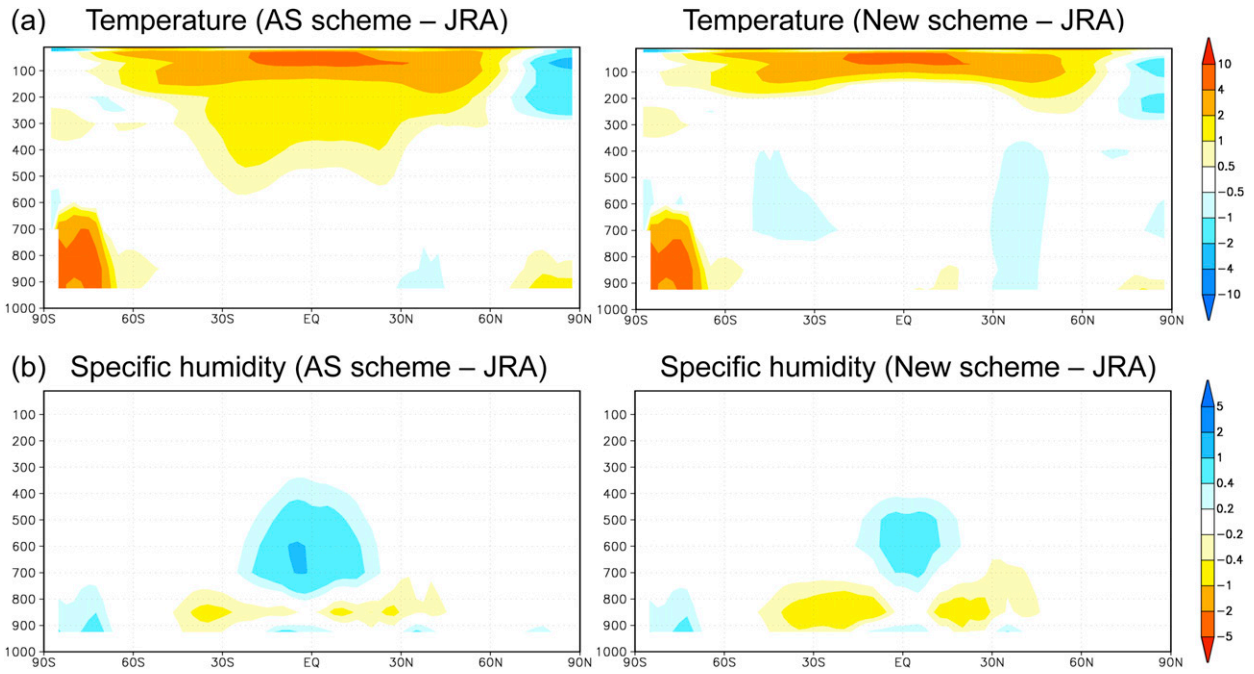

FIG. 8. Zonal mean annual mean climatology of 7-yr runs of the model using (left) the AS scheme and (right) the new scheme. (a) Difference in temperature between the models and JRA-25 (K day^{-1}). (b) Difference in specific humidity (g kg^{-1} day^{-1}) between the models and JRA-25.

overestimated. (However, this point is improved in the new AS-like scheme being developed in JMA.)

Figures 9b and 9c show the heating and moistening rates of the cumulus schemes. Corresponding to the difference in mass flux in Fig. 9a, heating and drying in the upper troposphere are larger in the AS scheme. The warm bias in the tropical upper troposphere in the AS scheme simulation seems to result from the large mass flux and heating in the upper troposphere. Figures 9d and 9e show the heating and moistening rates for the large-scale condensation scheme (Tiedtke cloud scheme). The simulations with the two cumulus schemes give substantially different results in the upper troposphere: positive heating and negative moistening rates in the new cumulus scheme simulation, and negative heating and positive moistening rates in the AS scheme simulation. This difference can be explained by the following equation in Tiedtke (1993):

$$\frac{dq_s}{dt} = \left(\frac{dq_s}{dp}\right)_{\text{ma}} (\omega + gM_c) + \frac{dq_s}{dT}\left(\frac{dT}{dt}\right)_{\text{diab}}, \quad (44)$$

where q_s is the saturation specific humidity, $M_c = \dot{M}_u + \dot{M}_d$ represents the compensatory subsidence (see appendix F for the calculation of $\dot{M}_u$ and $\dot{M}_d$), $\omega = dp/dt$ represents the grid-scale vertical velocity, $(dq_s/dp)_{\text{ma}}$ is the change in q_s accompanying the change of pressure and temperature constrained to lie on a moist adiabat, and $(dT/dt)_{\text{diab}}$ represents the change of temperature by radiative and turbulent processes, etc. In the typical convective regions in the tropics, there are grid-scale upward motions, so ω is negative. Since gM_c is positive, the sign of $\omega + gM_c$ depends on whether ω or gM_c has the larger absolute value. Figure 10 shows the simulated June–July–August climatologies of gM_c and $\omega + gM_c$ in the active regions of convections. In the new cumulus scheme simulation, negative $\omega + gM_c$ is likely in the tropical upper troposphere because of small M_c, which leads to $dq_s/dt < 0$ from Eq. (44), and heating and drying by the large-scale condensation. In contrast, in the AS scheme simulation, $\omega + gM_c > 0$ is likely in the tropical upper troposphere due to large M_c, which leads to $dq_s/dt > 0$, resulting in cooling and moistening by the evaporation of cloud water. It is difficult to say which is better; however, the results of the new cumulus scheme are closer to the following description in Johnson and Young (1983), "Mesoscale anvils, defined as widespread (~100 km) cloud systems extending from near the freezing level to the upper troposphere, are characterized by light stratiform precipitation," and the descriptions in other papers (e.g., Leary and Houze 1979; Johnson 1984).

6. Model variability

The Wheeler–Kiladis diagrams (Wheeler and Kiladis 1999; Kim et al. 2009) are shown in Fig. 11, which shows zonal wavenumber–frequency power spectra of symmetric and antisymmetric components of OLR divided

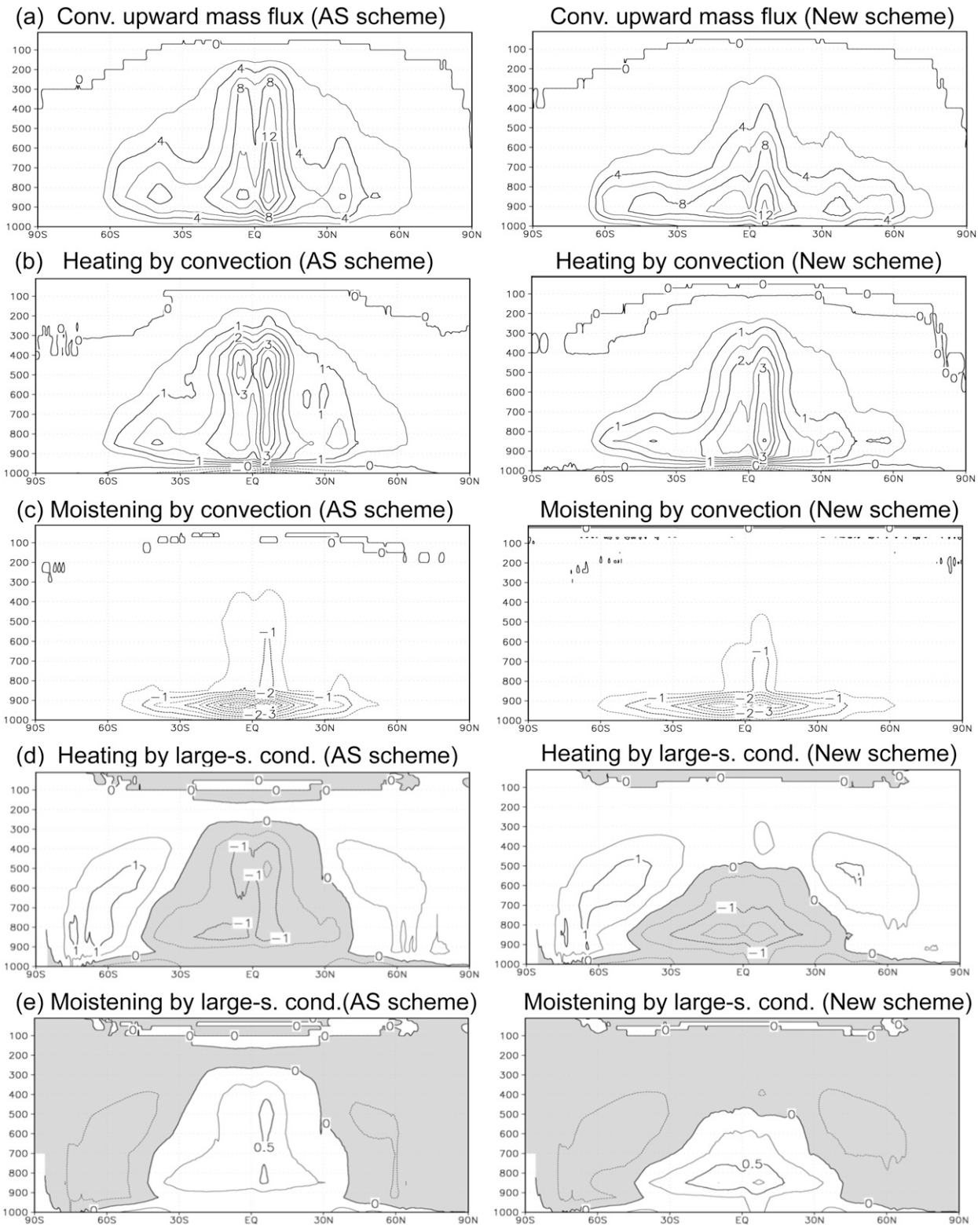

FIG. 9. As in Fig. 8, but for (a) convective updraft mass flux (g kg^{-1} day^{-1}), (b) heating by cumulus scheme (K day^{-1}), (c) moistening by cumulus scheme (g kg^{-1} day^{-1}), (d) heating by large-scale condensation scheme (K day^{-1}), and (e) moistening by large-scale condensation scheme (g kg^{-1} day^{-1}). Negative regions are shaded in (d) and (e).

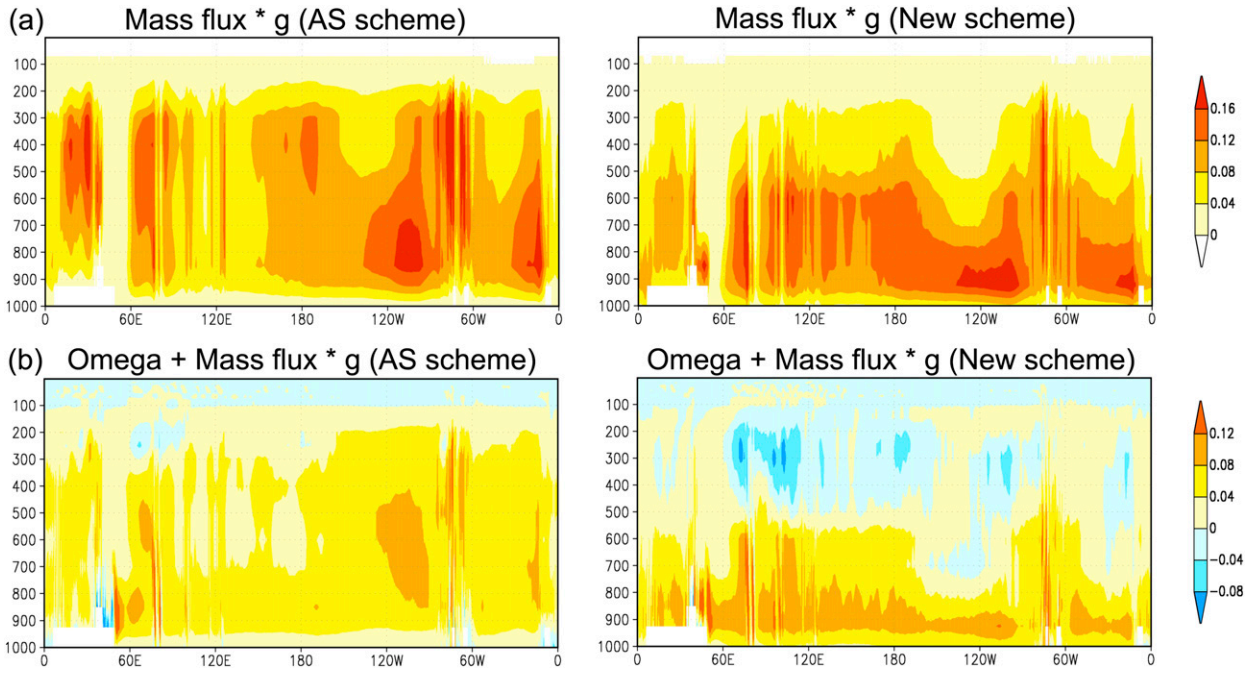

FIG. 10. Longitude–vertical cross section averaged between 5° and 10°N of June–July–August climatology of the 7-yr runs using (left) the AS scheme and (right) the new scheme. (a) Compensatory subsidence multiplied by gravity acceleration, gM_c (Pa s^{-1}). (b) Grid-scale vertical velocity plus (a), $\omega + gM_c$ (Pa s^{-1}).

by the background power. The Advanced Very High Resolution Radiometer (AVHRR) OLR observation data (Liebmann and Smith 1996) are used to compare with the model results. The result of not only AVHRR 26-yr data from 1979 to 2005 but also 7-yr data from 1999 to 2005 is shown to compare 7-yr model results. The Madden–Julian oscillation (MJO) signal in the period of 30–80 days in the new cumulus scheme simulation is clearer than that in the AS scheme simulation, but their signals are still weaker than the observation. However, the latest version of MRI-AGCM (v3.3) used in MRI-CGCM3 (Yukimoto et al. 2012), where the new cumulus scheme with different tuning parameters and the two-moment bulk cloud scheme are used, shows good results in MJO predictions (N. P. Klingaman et al. 2014, manuscript submitted to *J. Geophys. Res.*; E. Shindo 2014, personal communication). The signal of the Kelvin waves in the AS scheme is larger than that of the new scheme, but their signals are weaker than the observation. The signals of $n = 1$ equatorical Rossby (ER) waves in the AS and the new schemes are good compared with the observation. The signals of $n = 0$ eastward inertia–gravity (EIG) waves in both schemes are very weak.

7. Estimation of computational costs of cumulus schemes

The whole computational time of the one-month runs of the models using AS scheme and the new scheme at the 60-km resolution (TL319L64) is about 11 480 and 11 280 s, respectively, when one node (16 processors of IBM Power 6) of Hitachi SR16000 supercomputer is used. The computational time of the AS scheme part and the new scheme part per one-month run is about 731 and 834 s, respectively, as shown in Table 1. When the AS scheme is used, the calculation of dynamic CAPE generation rate (DCAPE; Xie and Zhang 2000; Nakagawa 2008) and the horizontal advection of cloud-base mass fluxes are additionally executed, so the whole computational time of the one-month runs of the AS scheme model is larger than that of the new scheme model.

The computational time of other types of cumulus schemes are also estimated in Table 1. In the computational time of the new scheme, the time of the part where the computational time becomes twice by calculating two convective updraft mass fluxes and that of the rest part are about 50/50. Therefore, when the number M of the multiple updraft mass fluxes are explicitly calculated, the computational time are roughly estimated to become about $0.5 + 0.25\,M$ times as long as that of the new scheme as shown in Table 1. The computational time in the Tiedtke-type schemes is estimated to be about 0.75 times as long as that in the new scheme by substituting $M = 1$. The computational time in the cumulus scheme explicitly calculating almost all (some) updraft mass fluxes layer by layer is roughly estimated to

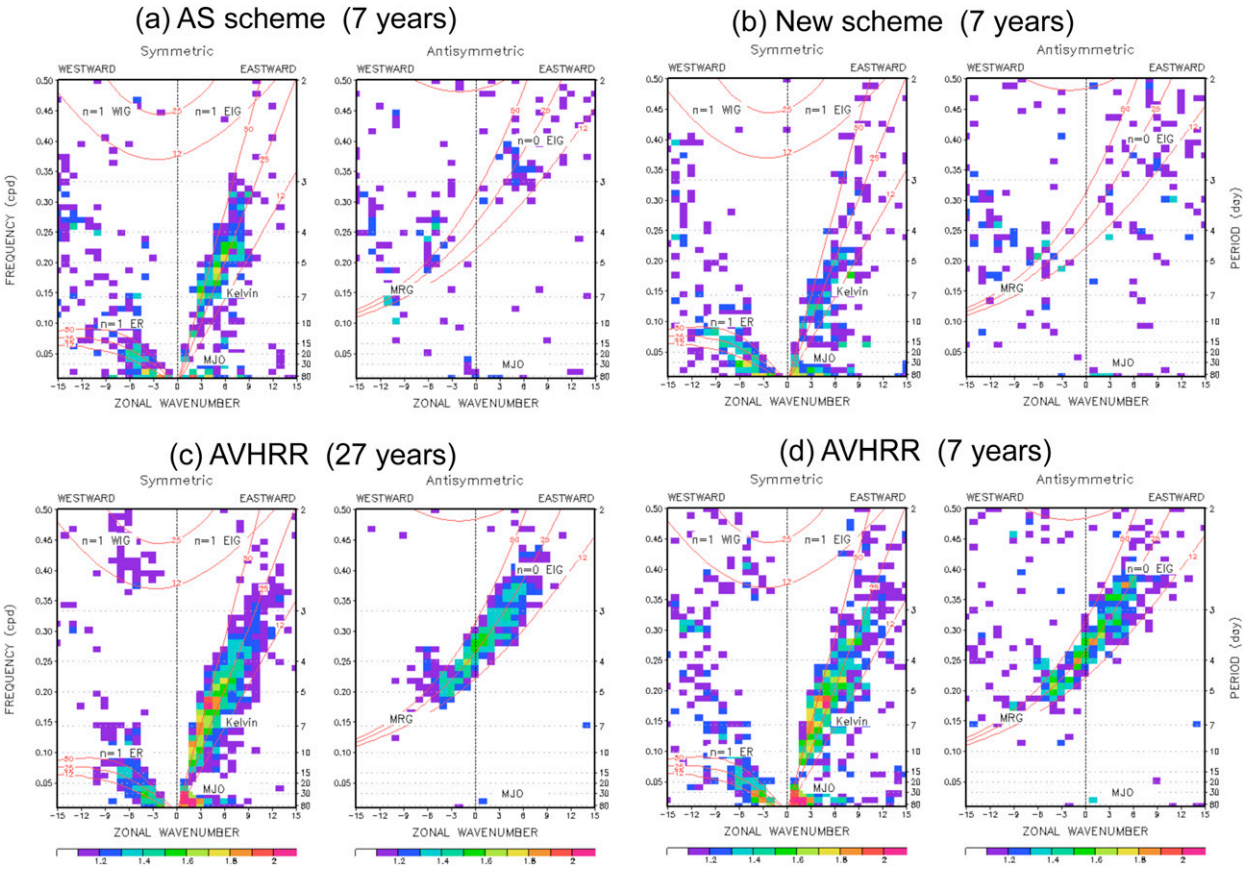

FIG. 11. Wheeler–Kiladis diagrams: zonal wavenumber–frequency power spectra of symmetric and antisymmetric components of OLR divided by the background power, for (a) the 7-yr run using the AS scheme, (b) the 7-yr run using the new cumulus scheme, (c) the 27-yr AVHRR observation from January 1979 to December 2005, and (d) the 7-yr AVHRR observation from January 1999 to December 2005.

be 7 (3) times as long as that in the new scheme, for example, when $M = 26$ ($M = 10$).

8. Summary and conclusions

We have developed a new cumulus scheme that explicitly represents multiple cumulus clouds with different cloud tops by interpolating between two convective updrafts with large and small entrainment rates. The two convective updrafts are explicitly calculated and the variables (e.g., temperature and specific humidity) in convective updrafts with intermediate entrainment rates are obtained by linear interpolation. The new scheme has the advantage of the AS-type scheme in that the effects of multiple cumulus clouds are represented explicitly, and the advantage of the Tiedtke-type scheme in that in-cloud variables are calculated layer by layer.

In this scheme, a conservative and monotonic semi-Lagrangian scheme with the PRM interpolation profile is adopted to calculate the vertical transport by convection-induced compensatory subsidence. This relaxes the mass-flux limit due to the CFL condition, and ensures nonnegative natural material transport.

The results of this scheme are equivalent to those of a 26-member ensemble mean, in which each member has one of 26 equally spaced different entrainment rates. The new scheme, whose computational cost is much lower than that of the explicit 26-member calculation,

TABLE 1. Computational time of the AS scheme and the new scheme per one-month run, and computational time of the M-mass-flux-type scheme roughly estimated from that of the new scheme, where M is the number of the calculated updraft mass fluxes. Estimated time in cases of $M = 1$, $M = 10$, and $M = 26$ is also shown. Values in brackets are the ratio of the time to that of the new scheme.

AS scheme	New scheme (two mass fluxes)	M-mass-flux scheme	$M = 1$	$M = 10$	$M = 26$
731 s (0.84)	874 s (1.0)	$437 + 218.5M$ s $(0.5 + 0.25M)$	655.5 s (0.75)	2622 s (3.0)	6118 s (7.0)

can produce equivalent results. Rough estimation of the computational time of the cumulus scheme explicitly calculating 26 convective updrafts layer by layer is about 7 times as that of the new scheme.

The climatologies of precipitation distribution and zonal mean temperature in the model using the new scheme are closer to the observations than in the model using the AS scheme. In the AS scheme, the mass flux in the tropical upper troposphere is larger than in the new scheme, which seems to be related to the warm bias there.

The simulation of MJO in the new scheme is slightly better than in the AS scheme, and the latest version of MRI-AGCM shows good results in MJO predictions. The signals of $n = 0$ EIG waves in both schemes are very weak. We will try to improve the variability by modifying entrainment or closure assumption, etc., by referring to the papers describing entrainment (e.g., de Rooy et al. 2013) and the cumulus schemes showing good results in variability (e.g., Bechtold et al. 2008; Chikira and Sugiyama 2010).

Acknowledgments. We are grateful to Masato Sugi, Tomoaki Ose, Seiji Yukimoto, Yoshinori Yamada, Eiki Shindo, MRI model development members, and MRI model analysis members for providing important information about cumulus parameterization and MJO, evaluating the cumulus scheme, and encouraging us. This work was conducted under the framework of the "Development of Basic Technology for Risk Information on Climate Change" supported by the SOUSEI Program of the Ministry of Education, Culture, Sports, Science, and Technology of Japan. Figure 11 was made with a diagnostic tool developed by the U.S. CLIVAR MJO Working Group.

APPENDIX A

Discretization of Convective Updrafts

Variables such as T, q, l, u, and v are located at the full levels k; $k = 1$ is the lowest full level. The half level $k - 1/2$ is located at the boundary between the full levels $k - 1$ and k.

Equation (17) is discretized as

$$(\tilde{M}_u)_k = (\tilde{M}_u)_{k-1} + (\tilde{E}_u^{\mathrm{org}}\Delta z)_{k-1} - (\tilde{D}_u^{\mathrm{org}}\Delta z)_k, \tag{A1}$$

where $(\Delta z)_k = z_{k+1/2} - z_{k-1/2}$. Equation (A1) is calculated by dividing it into two steps as follows:

$$(\tilde{M}'_u)_k = (\tilde{M}_u)_{k-1} + (\tilde{E}_u^{\mathrm{org}}\Delta z)_{k-1}, \quad \text{and} \tag{A2}$$

$$(\tilde{M}_u)_k = (\tilde{M}'_u)_k - (\tilde{D}_u^{\mathrm{org}}\Delta z)_k. \tag{A3}$$

The relation between $(\tilde{M}'_u)_k$ and $(\tilde{M}_u)_k$ and the mass flux of each cloud type is shown in Fig. 2b. The variable $(\tilde{D}_u^{\mathrm{org}}\Delta z)_k$ is calculated from

$$(\tilde{D}_u^{\mathrm{org}}\Delta z)_k = \delta_k(\tilde{M}'_u)_k, \tag{A4}$$

where δ_k is obtained from Eq. (A11) below.

Equation (2) is discretized as

$$\begin{aligned}(\tilde{M}'_u)_k(s_u^{[a]})_k = {} & \{(\tilde{M}_u)_{k-1} - (\tilde{D}_u^{\mathrm{trb[a]}}\Delta z)_{k-1}\}(s_u^{[a]})_{k-1} \\ & + (\tilde{E}_u^{\mathrm{org}}\Delta z + \tilde{E}_u^{\mathrm{trb[a]}}\Delta z)_{k-1}(\bar{s})_{k-1} \\ & + (L\tilde{c}_u^{[a]}\bar{\rho}\Delta z)_k + \{(L_{\mathrm{subl}} - L_{\mathrm{vap}})\tilde{f}_u^{[a]}\bar{\rho}\Delta z\}_k,\end{aligned} \tag{A5}$$

$$\begin{aligned}(\tilde{M}'_u)_k(s_u'^{[b]})_k = {} & \{(\tilde{M}_u)_{k-1} - (\tilde{D}_u^{\mathrm{trb[b]}}\Delta z)_{k-1}\}(s_u^{[b]})_{k-1} \\ & + (\tilde{E}_u^{\mathrm{org}}\Delta z + \tilde{E}_u^{\mathrm{trb[b]}}\Delta z)_{k-1}(\bar{s})_{k-1} \\ & + (L\tilde{c}_u^{[b]}\bar{\rho}\Delta z)_k + \{(L_{\mathrm{subl}} - L_{\mathrm{vap}})\tilde{f}_u^{[b]}\bar{\rho}\Delta z\}_k,\end{aligned} \tag{A6}$$

and

$$(s_u^{[b]})_k = (1 - \delta_k)(s_u'^{[b]})_k + \delta_k(s_u^{[a]})_k. \tag{A7}$$

In Eq. (A7), $(s_u^{[b]})_k$ is obtained by linear interpolation of $(s_u^{[a]})_k$ and $(s_u'^{[b]})_k$ (see Fig. 2a). The variables $(q_u^{[a]})_k$, $(q_u'^{[b]})_k$, $(q_u^{[b]})_k$, $(l_u^{[a]})_k$, $(l_u'^{[b]})_k$, $(l_u^{[b]})_k$, $(l_u^{\mathrm{ice[a]}})_k$, $(l_u'^{\mathrm{ice[b]}})_k$, and $(l_u^{\mathrm{ice[b]}})_k$ are calculated from the equations obtained by discretizing Eqs. (3)–(5) similarly. Condensation ($\tilde{c}_u^{[a]}$ and $\tilde{c}_u^{[b]}$) occurs when convective updrafts are saturated.

The coefficients $(\lambda_u^{[a]})_k$ and $(\lambda_u^{[b]})_k$ in Eqs. (12) and (13) are given by

$$\begin{cases} (\lambda_u^{[a]})_k = (\lambda_u^{[b]})_k = \lambda_{u,\mathrm{blwLCL}} & \text{when} \quad k < k_{\mathrm{LCL}} \\ (\lambda_u^{[a]})_k = (\lambda_u^{[b]})_k = \lambda_{u,\mathrm{blwLFC}} & \text{when} \quad k_{\mathrm{LCL}} \le k < k_{\mathrm{LFC}} \\ (\lambda_u^{[a]})_k = \lambda_{u,\min}, \quad (\lambda_u^{[b]})_k = \lambda_{u,\max} & \text{when} \quad k = k_{\mathrm{LFC}} \\ (\lambda_u^{[a]})_k = \lambda_{u,\min}, \quad (\lambda_u^{[b]})_k = \chi_k\lambda_{u,\max} + (1 - \chi_k)\lambda_{u,\min} & \text{when} \quad k_{\mathrm{LFC}} < k \end{cases}, \tag{A8}$$

where k_{LCL} is the lowest vertical level of condensation and k_{LFC} is the lowest vertical level of positive buoyancy. The values of $\lambda_{u,\min}$ and $\lambda_{u,\max}$ are given in Eqs. (14) and (15). We use the values

$$\lambda_{u,\ \mathrm{blwLCL}} = 0.0, \quad \text{and} \tag{A9}$$

$$\lambda_{u,\mathrm{blwLFC}} = 2.0 \times 10^{-4}. \tag{A10}$$

Equation (A12) below gives χ_k. The vertical distributions of $\lambda_u^{[\mathrm{a}]}$ and $\lambda_u^{[\mathrm{b}]}$ are shown in Fig. 2a.

The virtual temperatures $(T_{v,u})_k$ in convective updrafts with entrainment rates between $(\lambda_u^{[\mathrm{a}]})_k$ and $(\lambda_u^{[\mathrm{b}]})_{k-1}$ are assumed to be obtained by linear interpolation of $(T_{v,u}^{[\mathrm{a}]})_k$ and $(T_{v,u}^{\prime[\mathrm{b}]})_k$. When the virtual temperatures $(T_{v,u})_k$ in a part of the convective updrafts fall below the environmental virtual temperature $(\overline{T}_v)_k$, that part of the convective updrafts is detrained as organized detrainment (see Fig. 2). The proportion of detrainment δ_k is obtained by

$$\delta_k = \begin{cases} 1.0 & \text{when} \quad (T_{v,u}^{\prime[\mathrm{a}]})_k \le (\overline{T}_v)_k \\ \dfrac{(\overline{T}_v)_k - (T_{v,u}^{\prime[\mathrm{b}]})_k}{(T_{v,u}^{\prime[\mathrm{a}]})_k - (T_{v,u}^{\prime[\mathrm{b}]})_k} & \text{when} \quad (T_{v,u}^{\prime[\mathrm{b}]})_k < (\overline{T}_v)_k < (T_{v,u}^{\prime[\mathrm{a}]})_k \\ 0.0 & \text{when} \quad (\overline{T}_v)_k \le (T_{v,u}^{\prime[\mathrm{b}]})_k. \end{cases} \tag{A11}$$

The position of $(\lambda_u^{[\mathrm{b}]})_k$ between $\lambda_{u,\min}$ and $\lambda_{u,\max}$, χ_k, is obtained from

$$\chi_k = \begin{cases} 1.0 & \text{when} \quad k \le k_{\mathrm{LFC}} \\ (1-\delta_k)\chi_{k-1} & \text{when} \quad k_{\mathrm{LFC}} < k, \end{cases} \tag{A12}$$

and s, q, l, and l^{ice} in the organized detrainment are obtained from

$$(X_u^{\mathrm{orgdet}})_k = \frac{(X_u^{\prime[\mathrm{b}]})_k + (X_u^{[\mathrm{b}]})_k}{2}, \tag{A13}$$

where $X = s$, q, l, and l^{ice}.

APPENDIX B

Discretizing the Closure Assumption

To obtain $\mathrm{CAPE}^{(i)}$ in Eq. (26), $(\mathrm{CAPE}^{[\mathrm{a}]})_k$ and $(\mathrm{CAPE}^{[\mathrm{b}]})_k$, which are the CAPE of cumulus [a] and cumulus [b] up to the vertical level k, respectively, are calculated from

$$\begin{cases} (\mathrm{CAPE}^{[\mathrm{a}]})_k = (\mathrm{CAPE}^{[\mathrm{b}]})_k = 0 & \text{when} \quad k \le k_{\mathrm{LFC}} \\ \begin{cases} (\mathrm{CAPE}^{[\mathrm{a}]})_k = (\mathrm{CAPE}^{[\mathrm{a}]})_{k-1} + \dfrac{g}{(\overline{T}_v)_{k-1}}(T_{v,u}^{[\mathrm{a}]} - \overline{T}_v)_{k-1}(\Delta z)_{k-1} \\ (\mathrm{CAPE}^{\prime[\mathrm{b}]})_k = (\mathrm{CAPE}^{[\mathrm{b}]})_{k-1} + \dfrac{g}{(\overline{T}_v)_{k-1}}(T_{v,u}^{[\mathrm{b}]} - \overline{T}_v)_{k-1}(\Delta z)_{k-1} \\ (\mathrm{CAPE}^{[\mathrm{b}]})_k = (1-\delta_k)(\mathrm{CAPE}^{\prime[\mathrm{b}]})_k + \delta_k(\mathrm{CAPE}^{[\mathrm{a}]})_k \end{cases} & \text{when} \quad k > k_{\mathrm{LFC}}. \end{cases} \tag{B1}$$

$\mathrm{CAPE}^{(i)}$ is obtained from

$$\mathrm{CAPE}^{(i)} = \frac{(\mathrm{CAPE}^{\prime[\mathrm{b}]})_i + (\mathrm{CAPE}^{[\mathrm{b}]})_i}{2}. \tag{B2}$$

The decrease in $\mathrm{CAPE}^{(i)}$ due to the convective updraft of the cloud type (i) is obtained from

$$\left(\frac{\partial \mathrm{CAPE}}{\partial t}\right)^{(i)} \cong -\int_{\mathrm{cloud}(i)} \left(\frac{g}{\overline{T}_v}\frac{\partial \overline{T}_v}{\partial t}\right)^{(i)} dz \cong -\int_{\mathrm{cloud}(i)} \left(\frac{1}{c_p \overline{T}}\frac{\partial \overline{s}}{\partial z} + 0.608\frac{\partial \overline{q}}{\partial z}\right) M_u^{(i)} \frac{g\,dz}{\overline{\rho}}, \tag{B3}$$

where $\int_{\text{cloud}(i)} dz$ is the vertical integral up to the vertical level $k = i$.

The variable $(\tilde{M}_u^*)_k$ is defined as the provisional upward mass flux when it is assumed that organized detrainment does not occur. Then, $(\tilde{M}_u^*)_k$ is obtained from

$$(\tilde{M}_u^*)_k = \frac{(\tilde{M}_u)_k}{\chi_k} \tag{B4}$$

(see Fig. 2b). Organized entrainment is independent of cloud type (i), and the turbulent entrainment and the turbulent detrainment have the same value and do not affect the magnitude of the mass flux. So, $\tilde{\sigma}^{(i)}$ in Eq. (21) satisfies

$$\tilde{\sigma}^{(i)} = \frac{(\tilde{M}_u^{(i)})_k}{(\tilde{M}_u^*)_k}, \tag{B5}$$

not only at the level $k = k_{\text{LFC}}$, but also at the vertical levels $k > k_{\text{LFC}}$. It is assumed to be satisfied at the levels $k < k_{\text{LFC}}$ (see Figs. 2a,b). From Eqs. (22), (26), (B3), and (B5),

$$\alpha^{(i)} = \frac{\max(\text{CAPE}^{(i)} - \text{CIN}, \text{CAPE}^{(i)} \times 0.3)}{\tau \int_{\text{cloud}(i)} \left(\frac{1}{c_p \overline{T}} \frac{\partial \overline{s}}{\partial z} + 0.608 \frac{\partial \overline{q}}{\partial z} \right) \tilde{M}_u^* \frac{g\, dz}{\overline{\rho}}} \tag{B6}$$

is obtained.

Final (not provisional) values are obtained as follows. The organized detrainment is obtained from

$$(D_u^{\text{org}} \Delta z)_k = \alpha^{(k)} (\tilde{D}_u^{\text{org}} \Delta z)_k, \tag{B7}$$

while $(M_u)_k$ and $(M'_u)_k$ are calculated from the top level $k = k_{\text{top}}$ to the lower levels using the recurrence relation:

$$\beta_k = \begin{cases} 0 & \text{when} \quad k = k_{\text{top}} \\ \dfrac{(M'_u)_{k+1}}{(\tilde{M}'_u)_{k+1}} & \text{when} \quad k < k_{\text{top}}, \end{cases} \tag{B8}$$

$$(M_u)_k = \beta_k (\tilde{M}_u)_k, \quad \text{and} \tag{B9}$$

$$(M'_u)_k = (M_u)_k + (D_u^{\text{org}} \Delta z)_k. \tag{B10}$$

The variables $(E_u^{\text{org}})_k$, $(E_u^{\text{trb[a]}})_k$, $(E_u^{\text{trb[b]}})_k$, and $(D_u^{\text{trb[a]}})_k$, which are proportional to $(M_u)_k$, are also obtained by multiplying β_k with the provisional values as in Eq. (B9).

APPENDIX C

Discretization of the Convective Downdraft

Equations (27) and (28) are discretized, respectively, as

$$\begin{aligned} (-M_d)_k &= (-M_d)_{k+1} + (E_d^{\text{org}} \Delta z)_{k+1} + (E_d^{\text{trb}} \Delta z)_{k+1} - (D_d^{\text{trb}} \Delta z)_{k+1} - (D_d^{\text{org}} \Delta z)_k \\ &= (-M_d)_{k+1} + (E_d^{\text{org}} \Delta z)_{k+1} - (D_d^{\text{org}} \Delta z)_k, \quad \text{and} \end{aligned} \tag{C1}$$

$$\begin{aligned} \{-M_d + D_d^{\text{org}} \Delta z\}_k (s_d)_k &= (-M_d s_d)_{k+1} + (E_d^{\text{org}} \Delta z)_{k+1} (s_{\text{mix}})_{k+1} + (E_d^{\text{trb}} \Delta z)_{k+1} (\overline{s})_{k+1} - (D_d^{\text{trb}} \Delta z)_{k+1} (s_d)_{k+1} \\ &\quad - L(\overline{\rho} \Delta z)_{k+1} \{(e_d^{\text{cld}})_{k+1} + (e_d^{\text{prec}})_{k+1}\}. \end{aligned} \tag{C2}$$

Equation (29) is discretized in the same way as Eq. (28).

APPENDIX D

Discretization of Feedback to Environment

When calculating the effect of cumulus convection on the environment, the ensemble mean of the convective updrafts of the different cloud types, rather than the value of each cloud type (i), is necessary. Hereafter, $(\widehat{X}_u)_k$ is the ensemble mean of $(X_u^{(i)})_k$, and is calculated from

$$(\widehat{X}_u)_k = (1 - \gamma_k)(X_u^{[a]})_k + \gamma_k (X_u^{[b]})_k, \tag{D1}$$

where γ_k is calculated from the recurrence relation:

$$\gamma_k = \begin{cases} \dfrac{1}{2} & \text{when} \quad k = k_{\text{top}} \\ \dfrac{(M_u)_{k+1}\gamma_{k+1}(1.0-\delta_{k+1}) + (D_u^{\text{org}}\Delta z)_{k+1}(1.0-\delta_{k+1}/2)}{(M_u)_{k+1} + (D_u^{\text{org}}\Delta z)_{k+1}} & \text{when} \quad k < k_{\text{top}}. \end{cases} \tag{D2}$$

Equation (D2) for the case $k < k_{\text{top}}$ is derived by comparing the equation

$$(\widehat{X}_u')_{k+1} = (1-\gamma_k)(X_u^{[a]})_{k+1} + \gamma_k(X_u'^{[b]})_{k+1} \tag{D3}$$

with the equation obtained by substituting Eqs. (D1), (A13), and (A7) (where s is replaced with X) into

$$(\widehat{X}_u')_{k+1} = \frac{(M_u)_{k+1}(\widehat{X}_u)_{k+1} + (D_u^{\text{org}}\Delta z)_{k+1}(X_u^{\text{orgdet}})_{k+1}}{(M_u)_{k+1} + (D_u^{\text{org}}\Delta z)_{k+1}}. \tag{D4}$$

The variables D_u and E_u are obtained from

$$(D_u)_k \equiv \left\{\sum_i (D_u^{(i)})\right\}_k = (D_u^{\text{org}})_k + (1-\gamma_k)(D_u^{\text{trb[a]}})_k + \gamma_k(D_u^{\text{trb[b]}})_k, \quad \text{and} \tag{D5}$$

$$(E_u)_k \equiv \left\{\sum_i (E_u^{(i)})\right\}_k = (E_u^{\text{org}})_k + (1-\gamma_k)(E_u^{\text{trb[a]}})_k + \gamma_k(E_u^{\text{trb[b]}})_k. \tag{D6}$$

The ensemble means of the detrained properties from the convective updrafts of all cloud types, s_u^{det}, q_u^{det}, l_u^{det}, and $i_u^{\text{ice,det}}$, are obtained from

$$(D_u)_k(X_u^{\text{det}})_k \equiv \left\{\sum_i (D_u^{(i)}X_u^{(i)})\right\}_k = (D_u^{\text{org}})_k(X_u^{\text{orgdet}})_k + (1-\gamma_k)(D_u^{\text{trb[a]}})_k(X_u^{[a]})_k + \gamma_k(D_u^{\text{trb[b]}})_k(X_u^{[b]})_k, \tag{D7}$$

where $X = s$, q, l, or l^{ice}.

Only Eq. (39) is discretized below, but Eqs. (40)–(42) are discretized in the same way. Considering that s_{mix} is the average of $\bar{s}$ and s_u^{det}, and using Eqs. (D5)–(D7), Eq. (39) is discretized as

$$\left\{\frac{\bar{s}^+ - \bar{s}}{\Delta t}\right\}_k = \frac{1}{\bar{\rho}\Delta z}[\{(M_u+M_d)\bar{s}\}_{k+1/2} - \{(M_u+M_d)\bar{s}\}_{k-1/2}] + \frac{1}{\bar{\rho}}\left\{-E_u\bar{s} - E_d^{\text{org}}\frac{\bar{s}+s_u^{\text{det}}}{2} - E_d^{\text{trb}}\bar{s}\right\}_k$$
$$+ \frac{1}{\bar{\rho}}\{D_u s_u^{\text{det}} + (D_d^{\text{org}} + D_d^{\text{trb}})s_d\}_k + \{-L_{\text{vap}}e_{\text{prec}} - (L_{\text{subl}} - L_{\text{vap}})(e_{\text{snow}} + m_{\text{prec}} - f_{\text{prec}})\}_k, \tag{D8}$$

where $\bar{s}^+$ is the value of $\bar{s}$ after time integration with the cumulus scheme, and Δt is the time step. By using the following definitions:

$$\Delta p \equiv \bar{\rho} g\,\Delta z\ (= p_{k-1/2} - p_{k+1/2}), \tag{D9}$$

$$\Delta p^{\text{ent}} \equiv E_u g\,\Delta z\Delta t + \frac{E_d^{\text{org}} g\Delta z\Delta t}{2} + E_d^{\text{trb}} g\Delta z\Delta t, \tag{D10}$$

$$\Delta p_u^{\text{det}} \equiv D_u g\Delta z\Delta t - \frac{E_d^{\text{org}} g\Delta z\Delta t}{2}, \quad \text{and} \tag{D11}$$

$$\Delta p_d^{\text{det}} \equiv (D_d^{\text{org}} + D_d^{\text{trb}})g\Delta z\Delta t, \tag{D12}$$

Eq. (D8) is transformed into

$$\{\bar{s}^+\Delta p\}_k = \{\bar{s}(\Delta p - \Delta p^{\text{ent}})\}_k + \{(M_u+M_d)g\Delta t\bar{s}\}_{k+1/2} - \{(M_u+M_d)g\Delta t\bar{s}\}_{k-1/2} + \{s_u^{\text{det}}\Delta p_u^{\text{det}} + s_d\Delta p_d^{\text{det}}\}_k$$
$$+ [\{-L_{\text{vap}}e_{\text{prec}} - (L_{\text{subl}} - L_{\text{vap}})(e_{\text{prec}}^{\text{snow}} + m_{\text{prec}} - f_{\text{prec}})\}\Delta p\Delta t]_k. \tag{D13}$$

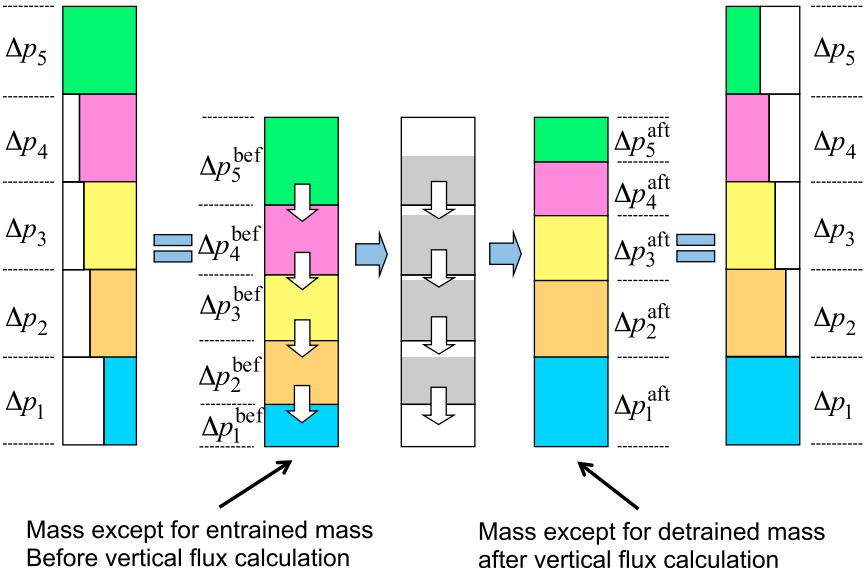

FIG. D1. Vertical transport of mass by compensatory subsidence. The gray area in the middle figure shows the mass moving from the upper layer to the lower layer.

The second and the third terms in Eq. (D13) represent the vertical flux by compensatory subsidence.

APPENDIX E

Semi-Lagrangian Calculation of Transport by Compensatory Subsidence

Figure D1 shows the vertical transport of mass along with the compensatory subsidence. In Fig. D1,

$$(\Delta p^{\rm bef})_k \equiv (\Delta p - \Delta p^{\rm ent})_k \tag{E1}$$

is the mass (multiplied by g) of the environment excluding the entrainment by cumulus convection, while

$$(\Delta p^{\rm aft})_k \equiv (\Delta p - \Delta p_u^{\rm det} - \Delta p_d^{\rm det})_k \tag{E2}$$

is the mass of the environment excluding the detrainment from cumulus convection. The vertical summation of the entrainment is equal to the vertical summation of the detrainment, so

$$\sum_k (\Delta p^{\rm bef})_k = \sum_k (\Delta p^{\rm aft})_k \tag{E3}$$

is satisfied. The gray area in the central part of Fig. D1 represents $\{(M_u + M_d)g\Delta t\}_{k+1/2}$, the mass moving from the upper layer $k+1$ to the lower layer k associated with the compensatory subsidence. Figure D2 shows the vertical flux of the variable X (such as s and q). Here, $(X^{\rm bef})_k$ in the left panel of Fig. D2 is the value before the vertical flux calculation. Using the piecewise rational method (PRM), an interpolation function $X = X(p)$ is obtained, where the mean value of $X(p)$ in layer k before the vertical flux calculation agrees with $(X^{\rm bef})_k$. Next, $(X^{\rm aft})_k$ is obtained by calculating the mean value of $X(p)$ in layer k after the vertical flux calculation (see the right panel of Fig. D2). The gray area in the central part of Fig. D2 represents $\{(M_u + M_d)g\Delta t\overline{X}\}_{k+1/2}$, the quantity of X moving from the upper layer $k+1$ to the lower layer k, and

$$(X^{\rm bef})_k(\Delta p^{\rm bef})_k + \{(M_u + M_d)g\Delta t\overline{X}\}_{k+1/2} - \{(M_u + M_d)g\Delta t\overline{X}\}_{k-1/2} = (X^{\rm aft})_k(\Delta p^{\rm aft})_k \tag{E4}$$

is satisfied. Here the conservation equations over the column

$$\sum_k (X^{\rm bef})_k(\Delta p^{\rm bef})_k = \sum_k (X^{\rm aft})_k(\Delta p^{\rm aft})_k \quad \left[= \int X(p)dp\right] \tag{E5}$$

are satisfied. From $s^{\rm bef} = \overline{s}$, and using Eqs. (E4), (E1), and (E2), Eq. (D13) is transformed to

$$\{\overline{s}^+\Delta p\}_k = \{s^{\rm aft}(\Delta p - \Delta p_u^{\rm det} - \Delta p_d^{\rm det})\}_k + \{s_u^{\rm det}\Delta p_u^{\rm det} + s_d\Delta p_d^{\rm det}\}_k + [\{-L_{\rm vap}e_{\rm prec} - (L_{\rm subl} - L_{\rm vap})(e_{\rm prec}^{\rm snow} + m_{\rm prec} - f_{\rm prec})\}\Delta p\Delta t]_k \tag{E6}$$

from which $\overline{s}^+$ is obtained.

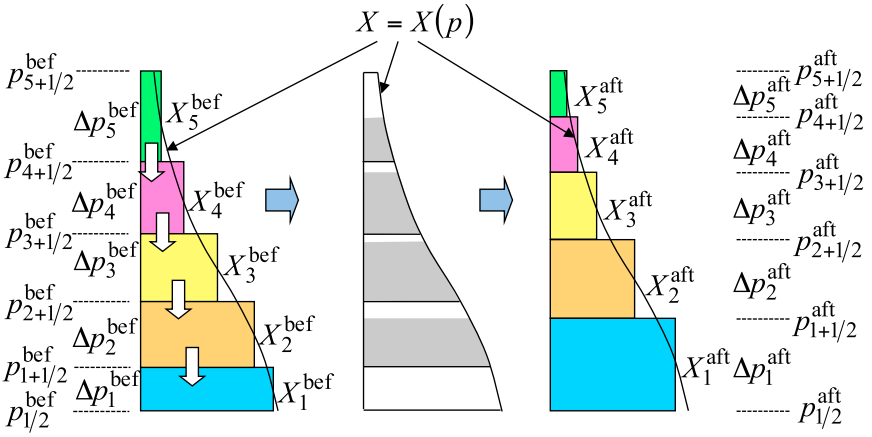

FIG. D2. Vertical transport of static energy, water vapor, etc., by compensatory subsidence. The gray area of the middle figure shows the quantity moving from the upper layer to the lower layer.

APPENDIX F

Values of Mass Flux at Half Levels and at Full Levels

The upward mass flux at the half level $k - 1/2$ is given by

$$(M_u)_{k-1/2} = (M'_u)_k, \tag{F1}$$

because $(M'_u)_k$ is the mass moving from the full level $k - 1$ to the full level k per unit time [see Eq. (A2)].

The downward mass flux in the convective downdraft at the half level $k - 1/2$ is given by

$$(-M_d)_{k-1/2} = (-M_d)_k + (E_d^{\text{org}}\Delta z)_k \tag{F2}$$

because $(-M_d)_{k+1} + (E_d^{\text{org}}\Delta z)_{k+1}$ in Eq. (C1) is the mass moving from the full level $k + 1$ to the full level k per unit time.

The mass fluxes at the full level k in Eq. (44) and in Figs. 3, 5, and 9 are obtained from

$$(\dot{M}_u)_k = \frac{(M_u)_{k+1/2} + (M_u)_{k-1/2}}{2}, \quad \text{and} \tag{F3}$$

$$(\dot{M}_d)_k = \frac{(M_d)_{k+1/2} + (M_d)_{k-1/2}}{2}. \tag{F4}$$

REFERENCES

Arakawa, A., and W. H. Schubert, 1974: Interaction of a cumulus cloud ensemble with the large-scale environment, Part I. *J. Atmos. Sci.,* **31,** 674–701, doi:10.1175/1520-0469(1974)031<0674:IOACCE>2.0.CO;2.

Bechtold, P., M. Köhler, T. Jung, F. Doblas-Reyes, M. Leutbecher, M. Rodwell, F. Vitart, and G. Balsamo, 2008: Advances in simulating atmospheric variability with the ECMWF model: From synoptic to decadal time-scales. *Quart. J. Roy. Meteor. Soc.,* **134,** 1337–1351, doi:10.1002/qj.289.

Betts, A. K., and M. J. Miller, 1986: A new convective adjustment scheme. Part II: Single column tests using GATE wave, BOMEX, ATEX and arctic air-mass data sets. *Quart. J. Roy. Meteor. Soc.,* **112,** 693–709, doi:10.1002/qj.49711247308.

Bryan, G. H., J. C. Wingaard, and J. M. Fritsch, 2003: Resolution requirements for the simulation of deep moist convection. *Mon. Wea. Rev.,* **131,** 2394–2416, doi:10.1175/1520-0493(2003)131<2394:RRFTSO>2.0.CO;2.

Chikira, M., and M. Sugiyama, 2010: A cumulus parameterization with state-dependent entrainment rate. Part I: Description and sensitivity to temperature and humidity profiles. *J. Atmos. Sci.,* **67,** 2171–2193, doi:10.1175/2010JAS3316.1.

Collins, W. D., 2001: Parameterization of generalized cloud overlap for radiative calculation in general circulation models. *J. Atmos. Sci.,* **58,** 3224–3242, doi:10.1175/1520-0469(2001)058<3224:POGCOF>2.0.CO;2.

de Rooy, W. C., and Coauthors, 2013: Entrainment and detrainment in cumulus convection: An overview. *Quart. J. Roy. Meteor. Soc.,* **139,** 1–19, doi:10.1002/qj.1959.

ECMWF, 2006: IFS documentation CY31r1. [Available online at http://nwmstest.ecmwf.int/research/ifsdocs/CY31r1/index.html.]

Eito, H., M. Murakami, C. Muroi, T. Kato, S. Hayashi, H. Kuroiwa, and M. Yoshizaki, 2010: The structure and formation mechanism of transversal cloud bands associated with the Japan-Sea polar-airmass convergence zone. *J. Meteor. Soc. Japan,* **88,** 625–648, doi:10.2151/jmsj.2010-402.

Emanuel, K. A., 1991: A scheme for representing cumulus convection in large-scale models. *J. Atmos. Sci.,* **48,** 2313–2335, doi:10.1175/1520-0469(1991)048<2313:ASFRCC>2.0.CO;2.

Endo, H., A. Kitoh, T. Ose, R. Mizuta, and S. Kusunoki, 2012: Future changes and uncertainties in Asian precipitation simulated by multi-physics and multi-sea surface temperature ensemble experiments with high-resolution Meteorological Research Institute atmospheric general circulation models (MRI-AGCMs). *J. Geophys. Res.,* **117,** D16118, doi:10.1029/2012JD017874.

Fritsch, J. M., and C. F. Chappell, 1980: Numerical prediction of convectively driven mesoscale pressure systems. Part I: Convective parameterization. *J. Atmos. Sci.,* **37,** 1722–1733, doi:10.1175/1520-0469(1980)037<1722:NPOCDM>2.0.CO;2.

Gravel, S., and A. Staniforth, 1994: A mass-conserving semi-Lagrangian scheme for the shallow-water equations. *Mon. Wea. Rev.,* **122,** 243–248, doi:10.1175/1520-0493(1994)122<0243:AMCSLS>2.0.CO;2.

Gregory, D., and P. Rowntree, 1990: A mass flux convection scheme with representation of cloud ensemble characteristics and stability-dependent closure. *Mon. Wea. Rev.,* **118,** 1483–1506, doi:10.1175/1520-0493(1990)118<1483:AMFCSW>2.0.CO;2.

——, R. Kershaw, and P. M. Inness, 1997: Parameterization of momentum transports by convection. II: Tests in single-column and general circulation models. *Quart. J. Roy. Meteor. Soc.,* **123,** 1153–1183, doi:10.1002/qj.49712354103.

Hu, Q., 1997: A cumulus parameterization based on a cloud model of intermittently rising thermals. *J. Atmos. Sci.,* **54,** 2292–2307, doi:10.1175/1520-0469(1997)054<2292:ACPBOA>2.0.CO;2.

JMA, 2007: Outline of the operational numerical weather prediction at the Japan Meteorological Agency (Appendix to WMO numerical weather prediction progress report). Japan Meteorological Agency, 194 pp. [Available online at http://www.jma.go.jp/jma/jma-eng/jma-center/nwp/outline-nwp/index.htm.]

Johnson, R. H., 1984: Partitioning tropical heat and moisture budgets into cumulus and mesoscale components: Implications for cumulus parameterization. *Mon. Wea. Rev.,* **112,** 1590–1601, doi:10.1175/1520-0493(1984)112<1590:PTHAMB>2.0.CO;2.

——, and G. S. Young, 1983: Heat and moisture budgets of tropical mesoscale anvil clouds. *J. Atmos. Sci.,* **40,** 2138–2147, doi:10.1175/1520-0469(1983)040<2138:HAMBOT>2.0.CO;2.

Kain, J. S., and J. M. Fritsch, 1990: A one-dimensional entraining/detraining plume model and its application in convective parameterization. *J. Atmos. Sci.,* **47,** 2784–2802, doi:10.1175/1520-0469(1990)047<2784:AODEPM>2.0.CO;2.

Kanada, S., M. Nakano, S. Hayashi, T. Kato, M. Nakamura, K. Kurihara, and A. Kitoh, 2008: Reproducibility of maximum daily precipitation amount over Japan by a high-resolution non-hydrostatic model. *SOLA,* **4,** 105–108, doi:10.2151/sola.2008-027.

Kawai, H., 2006: PDF cloud scheme and prognostic cloud scheme in JMA global model. CAS/JSC WGNE Research Activities in Atmospheric and Ocean Modeling, Rep. 36, Japan Meteorological Agency, 4.15–4.16. [Available online at http://www.mri-jma.go.jp/Dep/cl/cl1/members/kawai/Publications/ResActWGNE2006.pdf.]

——, 2013: Improvement of a stratocumulus scheme for mid-latitude marine low clouds. CAS/JSC WGNE Research Activities in Atmospheric and Ocean Modeling, Rep. 42, Japan Meteorological Agency, 4.03–4.04. [Available online at http://www.wcrp-climate.org/WGNE/BlueBook/2013/individual-articles/04_Kawai_Hideaki_ResActWGNE2013b.pdf.]

Kim, D., and Coauthors, 2009: Application of MJO simulation diagnostics to climate models. *J. Climate,* **22,** 6413–6436, doi:10.1175/2009JCLI3063.1.

Kuell, V., and A. Bott, 2009: Application of the hybrid convection parameterization scheme HYMACS to different meteorological situations. *Atmos. Res.,* **94,** 743–753, doi:10.1016/j.atmosres.2009.04.002.

Kuo, H. L., 1965: On formation and intensification of tropical cyclones through latent heat release by cumulus convection. *J. Atmos. Sci.,* **22,** 40–63, doi:10.1175/1520-0469(1965)022<0040:OFAIOT>2.0.CO;2.

——, 1974: Further studies of the parameterization of the influence of cumulus convection on large-scale flow. *J. Atmos. Sci.,* **31,** 1232–1240, doi:10.1175/1520-0469(1974)031<1232:FSOTPO>2.0.CO;2.

Leary, C. A., and R. A. Houze Jr., 1979: The structure and evolution of convection in a tropical cloud cluster. *J. Atmos. Sci.,* **36,** 437–457, doi:10.1175/1520-0469(1979)036<0437:TSAEOC>2.0.CO;2.

Liebmann, B., and C. A. Smith, 1996: Description of a complete (interpolated) outgoing longwave radiation dataset. *Bull. Amer. Meteor. Soc.,* **77,** 1275–1277.

Lilly, D. K., 1990: Numerical prediction of thunderstorms—Has its time come? *Quart. J. Roy. Meteor. Soc.,* **116,** 779–798, doi:10.1002/qj.49711649402.

Lin, S.-J., and R. B. Rood, 1996: Multidimensional flux-form semi-Lagrangian transport scheme. *Mon. Wea. Rev.,* **124,** 2046–2070, doi:10.1175/1520-0493(1996)124<2046:MFFSLT>2.0.CO;2.

Lindzen, R. S., 1988: Some remarks on cumulus parameterization. *Pure Appl. Geophys.,* **126,** 123–135, doi:10.1007/BF00876918.

Loeb, N. G., B. A. Wielicki, D. R. Doelling, G. L. Smith, D. F. Keyes, S. Kato, N. M. Smith, and T. Wong, 2009: Toward optimal closure of the earth's top-of-atmosphere radiation budget. *J. Climate,* **22,** 748–766, doi:10.1175/2008JCLI2637.1.

Lopez, P., and E. Moreau, 2005: A convection scheme for data assimilation: Description and initial tests. *Quart. J. Roy. Meteor. Soc.,* **131,** 409–436, doi:10.1256/qj.04.69.

Manabe, S., and R. F. Strickler, 1964: Thermal equilibrium of the atmosphere with a convective adjustment. *J. Atmos. Sci.,* **21,** 361–385, doi:10.1175/1520-0469(1964)021<0361:TEOTAW>2.0.CO;2.

Mizuta, R., and Coauthors, 2006: 20-km-mesh global climate simulations using JMA-GSM model—Mean climate states. *J. Meteor. Soc. Japan,* **84,** 165–185, doi:10.2151/jmsj.84.165.

——, and Coauthors, 2012: Climate simulations using the improved MRI-AGCM with 20-km grid. *J. Meteor. Soc. Japan,* **90A,** 233–258, doi:10.2151/jmsj.2012-A12.

Moorthi, S., and M. J. Suarez, 1992: Relaxed Arakawa–Schubert: A parameterization of moist convection for general circulation models. *Mon. Wea. Rev.,* **120,** 978–1002, doi:10.1175/1520-0493(1992)120<0978:RASAPO>2.0.CO;2.

Murakami, H., and Coauthors, 2012a: Future changes in tropical cyclone activity projected by the new high-resolution MRI-AGCM. *J. Climate,* **25,** 3237–3260, doi:10.1175/JCLI-D-11-00415.1.

——, R. Mizuta, and E. Shindo, 2012b: Future changes in tropical cyclone activity projected by multi-physics and multi-SST ensemble experiments using the 60-km-mesh MRI-AGCM. *Climate Dyn.,* **39,** 2569–2584, doi:10.1007/s00382-011-1223-x.

Nagasawa, R., 2012: The problem of cloud overlap in the radiation process of JMA's global NWP model. CAS/JSC WGNE Research Activities in Atmospheric and Ocean Modeling, Rep. 42, Japan Meteorological Agency, 4.15–4.16. [Available online at http://www.wcrp-climate.org/WGNE/BlueBook/2012/individual-articles/04_Nagasawa_Ryoji_04_Ryoji_Nagasawa_cloudoverlap.pdf.]

Nakagawa, M., 2008: Improvement of the cumulus parameterization scheme of the operational global NWP model at JMA. CAS/JSC WGNE Research Activities in Atmospheric and Ocean Modeling, Rep. 38, Japan Meteorological Agency, 4.09–4.10. [Available online at http://www.wcrp-climate.org/WGNE/BlueBook/2008/individual-articles/04_Nakagawa_Masayuki___30330.pdf.]

Nober, F. J., and H.-F. Graf, 2005: A new convective cloud field model based on principles of self-organization. *Atmos. Chem. Phys.,* **5,** 2749–2759, doi:10.5194/acp-5-2749-2005.

Nordeng, T. E., 1994: Extended versions of the convective parameterization scheme at ECMWF and their impact on the mean and transient activity of the model in the tropics. ECMWF Tech. Memo. 206, ECMWF, 41 pp.

Onogi, K., and Coauthors, 2007: The JRA-25 reanalysis. *J. Meteor. Soc. Japan,* **85,** 369–432, doi:10.2151/jmsj.85.369.

Pan, D., and D. Randall, 1998: A cumulus parameterization with a prognostic closure. *Quart. J. Roy. Meteor. Soc.,* **124,** 949–981, doi:10.1002/qj.49712454714.

Park, S., and C. S. Bretherton, 2009: The University of Washington shallow convection and moist turbulence schemes and their impact on climate simulations with the Community Atmosphere Model. *J. Climate,* **22,** 3449–3469, doi:10.1175/2008JCLI2557.1.

Posselt, D. J., S. C. van den Heever, and G. L. Stephens, 2008: Trimodal cloudiness and tropical stable layers in simulations of radiative convective equilibrium. *Geophys. Res. Lett.,* **35,** L08802, doi:10.1029/2007GL033029.

Priestley, A., 1993: A quasi-conservative version of the semi-Lagrangian advection scheme. *Mon. Wea. Rev.,* **121,** 621–629, doi:10.1175/1520-0493(1993)121<0621:AQCVOT>2.0.CO;2.

Raymond, D. J., and A. M. Blyth, 1986: A stochastic mixing model for nonprecipitating cumulus clouds. *J. Atmos. Sci.,* **43,** 2708–2718, doi:10.1175/1520-0469(1986)043<2708:ASMMFN>2.0.CO;2.

Reynolds, R. W., and T. M. Smith, 1994: Improved global sea surface temperature analysis using optimum interpolation. *J. Climate,* **7,** 929–948, doi:10.1175/1520-0442(1994)007<0929:IGSSTA>2.0.CO;2.

Satoh, M., T. Matsuno, H. Tomita, H. Miura, T. Nasuno, and S. Iga, 2008: Nonhydrostatic Icosahedral Atmospheric Model (NICAM) for global cloud resolving simulations. *J. Comput. Phys.,* **227,** 3486–3514, doi:10.1016/j.jcp.2007.02.006.

Smith, R. N. B., 1990: A scheme for prediction layer clouds and their water content in a general circulation model. *Quart. J. Roy. Meteor. Soc.,* **116,** 435–460, doi:10.1002/qj.49711649210.

Sundqvist, H., 1978: A parameterization scheme for non-convective condensation including precipitation of cloud water content. *Quart. J. Roy. Meteor. Soc.,* **104,** 677–690, doi:10.1002/qj.49710444110.

Taylor, K. E., 2001: Summarizing multiple aspects of model performance in a single diagram. *J. Geophys. Res.,* **106,** 7183–7192, doi:10.1029/2000JD900719.

Tiedtke, M., 1989: A comprehensive mass flux scheme for cumulus parameterization in large-scale models. *Mon. Wea. Rev.,* **117,** 1779–1800, doi:10.1175/1520-0493(1989)117<1779:ACMFSF>2.0.CO;2.

——, 1993: Representation of clouds in large-scale models. *Mon. Wea. Rev.,* **121,** 3040–3061, doi:10.1175/1520-0493(1993)121<3040:ROCILS>2.0.CO;2.

Wagner, T. M., and H. F. Graf, 2010: An ensemble cumulus convection parameterization with explicit cloud treatment. *J. Atmos. Sci.,* **67,** 3854–3869, doi:10.1175/2010JAS3485.1.

Wheeler, M., and G. N. Kiladis, 1999: Convectively coupled equatorial waves: Analysis of clouds and temperature in the wavenumber–frequency domain. *J. Atmos. Sci.,* **56,** 374–399, doi:10.1175/1520-0469(1999)056<0374:CCEWAO>2.0.CO;2.

Wood, R., and C. S. Bretherton, 2006: On the relationship between stratiform low cloud cover and lower tropospheric stability. *J. Climate,* **19,** 6425–6432, doi:10.1175/JCLI3988.1.

Wu, X., and M. Yanai, 1994: Effects of vertical wind shear on the cumulus transport of momentum: Observation and parameterization. *J. Atmos. Sci.,* **51,** 1640–1660, doi:10.1175/1520-0469(1994)051<1640:EOVWSO>2.0.CO;2.

Xiao, F., and X. Peng, 2004: A convexity preserving scheme for conservative advection transport. *J. Comput. Phys.,* **198,** 389–402, doi:10.1016/j.jcp.2004.01.013.

Xie, P., and P. A. Arkin, 1997: Global precipitation: A 17-year monthly analysis based on gauge observations, satellite estimates, and numerical model outputs. *Bull. Amer. Meteor. Soc.,* **78,** 2539–2558, doi:10.1175/1520-0477(1997)078<2539:GPAYMA>2.0.CO;2.

Xie, S., and M. Zhang, 2000: Impact of the convective triggering function on single-column model simulations. *J. Geophys. Res.,* **105,** 14 983–14 996, doi:10.1029/2000JD900170.

Yamasaki, M., 1975: A numerical experiment of the interaction between cumulus convection and large-scale motion. *Pap. Meteor. Geophys.,* **26,** 63–91.

Yanai, M., S. Esbensen, and J.-H. Chu, 1973: Determination of bulk properties of tropical cloud clusters from large-scale heat and moisture budgets. *J. Atmos. Sci.,* **30,** 611–627, doi:10.1175/1520-0469(1973)030<0611:DOBPOT>2.0.CO;2.

Yoshimura, H., and T. Matsumura, 2003: A semi-Lagrangian scheme conservative in the vertical direction. CAS/JSC WGNE Research Activities in Atmospheric and Ocean Modeling, Rep. 33, Japan Meteorological Agency, 3.19–3.20. [Available online at http://www.wcrp-climate.org/WGNE/BlueBook/2003/individual-articles/03-yoshimura.pdf.]

——, and ——, 2005: A two-time-level vertically-conservative semi-Lagrangian semi-implicit double Fourier series AGCM. CAS/JSC WGNE Research Activities in Atmospheric and Ocean Modeling, Rep. 35, Japan Meteorological Agency, 3.25–3.26. [Available online at http://www.wcrp-climate.org/WGNE/BlueBook/2005/individual-articles/03_Yoshimura_Hiromasa_03_yoshimura_hiromasa_2tl-dfs.pdf.]

——, and S. Yukimoto, 2008: Development of a Simple Coupler (Scup) for Earth System Modeling. *Pap. Meteor. Geophys.,* **59,** 19–29, doi:10.2467/mripapers.59.19.

Yukimoto, S., and Coauthors, 2011: Meteorological Research Institute-Earth System Model v1 (MRI-ESM1)—Model description. Tech. Rep. 64, Meteorological Research Institute, 88 pp.

——, and Coauthors, 2012: A new global climate model of the Meteorological Research Institute: MRI-CGCM3—Model description and basic performance. *J. Meteor. Soc. Japan,* **90A,** 23–64, doi:10.2151/jmsj.2012-A02.

Zhang, G., and N. McFarlane, 1995: Sensitivity of climate simulations to the parameterization of cumulus convection in the Canadian Climate Centre general circulation model. *Atmos.–Ocean,* **33,** 407–407, doi:10.1080/07055900.1995.9649539.